creative commons

COMMONS DEED

저작자표시-비영리-변경금지 2.0 대한민국

이용자는 아래의 조건을 따르는 경우에 한하여 자유롭게

- 이 저작물을 복제, 배포, 전송, 전시, 공연 및 방송할 수 있습니다.

다음과 같은 조건을 따라야 합니다:

저작자표시. 귀하는 원저작자를 표시하여야 합니다.

비영리. 귀하는 이 저작물을 영리 목적으로 이용할 수 없습니다.

변경금지. 귀하는 이 저작물을 개작, 변형 또는 가공할 수 없습니다.

- 귀하는, 이 저작물의 재이용이나 배포의 경우, 이 저작물에 적용된 이용허락조건을 명확하게 나타내어야 합니다.
- 저작권자로부터 별도의 허가를 받으면 이러한 조건들은 적용되지 않습니다.

저작권법에 따른 이용자의 권리는 위의 내용에 의하여 영향을 받지 않습니다.

이것은 이용허락규약(Legal Code)을 이해하기 쉽게 요약한 것입니다.

Disclaimer

dCollection

의학석사 학위논문

E-Cadherin 돌연변이 상태에 따른 위 종양 모델의 표현형 분석

Phenotypic Analysis of Gastric Tumor Models with Differential E-Cadherin Mutation Status

2023 년 8 월

서울대학교 대학원

의과학과 의과학전공

박 기 석

A thesis for the Degree of Master

E-Cadherin 돌연변이 상태에 따른 위 종양 모델의 표현형 분석

Phenotypic Analysis of Gastric Tumor Models with Differential E-Cadherin Mutation Status

July 2023

Department of Biomedical sciences, Seoul National University
College of medicine
Kiseok Park,

Phenotypic Analysis of Gastric Tumor Models with Differential E-Cadherin Mutation Status

지도 교수 정 기 훈

이 논문을 의학석사 학위논문으로 제출함
2023 년 4 월

서울대학교 대학원
의과학과 의과학전공
박 기 석

박기석의 의학석사 학위논문을 인준함
2023 년 7 월

위 원 장 _____ (인)

부위원장 _____ (인)

위 원 _____ (인)

Phenotypic Analysis of Gastric Tumor Models with Differential E-Cadherin Mutation Status

by

Kiseok Park

A thesis submitted to the Department of Biomedical Sciences in partial fulfillment of the requirements for the Degree of Master in Biomedical Sciences at Seoul National University College of Medicine

April 2023

Approved by Thesis Committee:
July 2023

Chair _____ (인)

Vice Chair _____ (인)

Examiner _____ (인)

Abstract

Gastric cancer(GC) is a major health concern with high mortality rates globally. Therapeutic options for gastric cancer include chemotherapy, immunotherapy and immune checkpoint blockade, however, limited response rates have been observed due to various factors, including tumor-protective microenvironment(TME). In this study, we investigated the distinct phenotypes of two murine gastric tumors, Tcon (Triple-conditional mutation) and Dcon(Double-conditional mutation. The results show that Tcon tumors, display severe desmoplasia characterized by the excessive accumulation of collagen fibers in the TME, which contributed to the stiffness and rigidity of the tumor mass. The desmoplastic reaction, facilitated by cancer-associated fibroblast(CAF)s, is a crucial factor in promoting tumor progression and hindering the delivery of therapeutic agents. My study also found that certain CAF subtypes, including αSMA single-positive CAFs, which contribute to tumor fibrosis, and CAFs expressing PD-L1, which may play a role in immunosuppression, were highly enriched in Tcon tumors compared to Dcon tumors. Furthermore, Tcon tumors exhibited compressed blood vessel with low functionality, indicating that Tcon tumors may exhibit lower therapy response rate due to worse drug delivery. Meanwhile, Dcon tumors displayed high immune cell infiltration, particularly $CD4^+$ and $CD8^+$ T cells producing TNFα, Granzyme B, Perforin and Interferon-γ, indicating that Dcon tumors possess potentials for better anti-tumor immunity than Tcon tumors. Additionally, Dcon tumor-bearing mice showed splenomegaly, enriched with myeloid cells and erythroblasts due to severe anemia. The enriched cells in the spleen were also expected to infiltrate into

Dcon tumors and exert immunosuppressive and/or pro-tumoral effects. Our findings provide important insights into the distinct phenotypes of two gastric tumors and clinical implications for improving the therapeutic accessibility of gastric cancer patients.

.....

Keyword : Gastric Cancer; Desmoplasia; Cancer-associated Fibroblast; Vascular compression; Splenomegaly
Student Number : 2021-23200

Table of Contents

INTRODUCTION

Gastric cancer is the fifth leading cause of cancer-related deaths worldwide in 2020 and sixth in cancer morbidity. It is highly prevalent in Asia, eastern Europe, and southern America, with consistently high mortality rates (1). According to Lauren's classification, GC is classified into two main types: intestinal and diffuse type. The intestinal type has a better prognosis and generally affects elderly males, exhibiting lymphatic or vascular invasion, while the diffuse type affects younger females, lacks adhesion, and features non-cohesive tumor cells that infiltrate the stroma (2). Additionally, Mixed Gastric Cancer (MGC), the third type of GC classification, is defined as possessing both diffuse and intestinal characteristics (3).

GC treatment includes chemotherapy, such as Oxaliplatin, Cisplatin, or 5-FU, immunotherapy, such as Trastuzumab that targets the HER2 receptor, and immune checkpoint blockade, such as Pembrolizumab and Nivolumab that induce T cell reinvigoration of the patient. However, the response rates to therapy and benefits for patients are currently limited (4,5). This phenomenon is due to the infiltration and functional activation of various cell types inside the tumor microenvironment (TME), such as immune cells, endothelial cells, and CAFs, as well as the therapy resistance and

anti-apoptotic characteristics that cancer cells originally possess. Therefore, a comprehensive and systematic analysis and profiling of TME is essential for clinical applications with higher efficacy (6,7,8).

CDH1 (E-Cadherin), found to be mutated in majority of hereditary diffuse gastric cancer patient, while Ras-RTK pathway alteration and p53 mutation are found in majority of GC patients. Till et al. studied the effect of CDH1 on tumorigenesis, overall survival, and metastasis (9). E-Cadherin is one of the epithelial adhesion molecules that belongs to the Cadherin family (10). Its well-characterized functions include physical attachment between epithelial cells, negative regulation of Wnt-signaling, including beta-catenin (12), and most importantly, tumor suppression (13). Recently, however, the function of soluble E-cadherin expressed on ovarian cancer cells and then cleaved by Matrix-metalloproteinase (MMP) has been discovered, of which significantly promotes tumor angiogenesis, seems to be quite opposite to its typical tumor suppressing functions (14).

Till et al. developed transgenic (TG) mice, termed Triple conditional mutant (Tcon) mouse (Atp4b-Cre; $Trp53^{fl/fl}$; LSL-$Kras^{G12D}$; $CDH1^{fl/fl}$; $Rosa26^{LSL-YFP}$) and double conditional mutant (Dcon) mouse with one copy of wild type-CDH1 (Atp4b-Cre; $Trp53^{fl/fl}$; LSL-$Kras^{G12D}$; $CDH1^{fl/+}$; $Rosa26^{LSL-YFP}$), to accurately reflect the mutational status of GC. The two types of TG mice showed different patterns of survival, metastasis, tumor growth, and tumorigenesis. Furthermore, the results of the microarray

analysis of Tcon and Dcon stomach showed that oncogenic Kras activity was increased and beta-catenin target genes were upregulated in Tcon stomach. This study produced a tumor model through subcutaneous injection in C57BL/6 mouse using Tcon and Dcon cell line derived from stomach of Tcon Dcon mouse in Till et al. I attempted to discover differences in the phenotypic characteristics of Tcon and Dcon tumor that were not covered in Till et al. Mice injected with Tcon tumor showed a bump after 7 days of injection, whereas Dcon tumor had a relatively slower tumorigenesis, confirming a pattern similar to the original article. (Till et al.) Furthermore, while the Tcon tumor was highly rigid and pale color, the Dcon tumor caught up with the growth of the Tcon tumor after 25 to 28 days of injection to exhibit fast tumor growth, with bloody color outside. In the case of Dcon tumor-bearing mice, extensive splenomegaly was observed, confirming that systematic effects were induced in the tumor macro-environment by Dcon tumor.

Among the subtypes of DGC, Scirrhous gastric cancer (SGC), known to have a poor prognosis, is accompanied by linitis plastica, which is a symptom of desmoplasia with the hardening and contraction of the stomach in which cancer-associated fibroblast (CAF)s act a decisive factor (15,16,17). Moreover, reports suggest that CAFs among the stromal cells of gastric tumors are activated by various secretory proteins derived from GC cells, producing ECM components such as collagen and fibronectin (18).

CAFs, initially discovered in desmoplastic breast cancers and

termed as Carcinoma-associated fibroblasts, are frequently found in tumor stroma as fibroblasts in an activated state (19). Furthermore, it has been reported that CAFs not only produce ECM components but also secrete pro-fibrotic growth factors such as TGF-β, PDGF, and FGF2 (20).

In the early days of discovery, CAFs were thought to be a homogeneous population of fibroblasts activated in tumor stroma, however, subsequent studies on various desmoplastic tumors, such as Pancreatic Ductal Adenocarcinoma (PDAC), have confirmed that CAFs are composed of heterogeneous subtypes (21). For example, Kim et al. defined six CAF subtypes in PDAC using scRNA-seq and discovered CAF-2, which is believed to be the major cause of desmoplastic reaction, and verified CD141 as a biomarker at the protein level (22). Additionally, Elyada et al. divided CAFs in PDAC into three subtypes: myofibroblastic-CAF (myCAF), inflammatory-CAF (iCAF), and antigen-presenting-CAF (apCAF), defining CAF subsets that not only induce desmoplasia but also modulate tumor immunity (23). Bartoschek et al. identified CAF subsets involved in angiogenesis, ECM production, and other functions in breast cancer (24).

While the main source of CAFs is resident fibroblasts, which generally exist at the site of tumor occurrence, it has been discovered that CAFs have various cellular origins or lineages (25). Reports suggest that epithelial cells, including carcinoma cells, can change into fibroblasts through Epithelial-to-mesenchymal transition (EMT) (26,27). In some desmoplastic tumors, including

PDAC, it has been reported that bone marrow-derived mesenchymal stem cells (MSCs) home to the tumor site to improve tumor progression and drug resistance, and MSCs have also been identified as a source of CAFs (28,29). Other cell types, including endothelial cells (30), adipocytes (31), mesothelial cells (32,33), pericytes (34), and even monocytes, have been reported to differentiate into CAFs, indicating the variety of cellular origins of CAFs (35).

CAFs are known to affect tumor progression through various pathways. Unlike resting or quiescent fibroblasts, fibroblasts activated by certain stimuli to produce ECM protein are called myofibroblasts or activated fibroblasts, which are the main causes of tumor fibrosis and proactive accumulation of ECM compound in the tumor stroma (36,37). Additionally, CAFs have been shown to not only inhibit drug delivery to the tumor through ECM accumulation but also secrete various proteins that enhance cancer cell survival and resistance to radiotherapy, chemotherapy, and immunotherapy by modulating host immune system (38,39).

In SGC, CAFs deliver pro-tumoral factors to cancer cells through $CD9^+$ exosomes, which have been shown to promote GC cell motility and metastasis via enzymes such as MMP2 and MMP11 (40,41). Moreover, CAFs are also known to promote GC cell invasion and metastasis by delivering various microRNAs (miRNAs) to cancer cells (42,43). In case of iCAF, a CAF subtype identified in PDAC, it not only secretes cytokines such as IL-6 and CXCL12 to induce immunosuppression in the tumor microenvironment (TME)

but has also been found to promote tumor immune evasion by inducing Treg differentiation and activation with an antigen-dependent mechanism (23,33). On the other hand, some CAFs have been reported to suppress tumor progression, unlike the tumor-promoting functions described above (44).

The formation of blood vessels through angiogenesis can also impact tumor progression in addition to CAFs. To satisfy the nutrient and oxygen demands required for cancer cell growth and proliferation, the tumor secretes several factors that induce angiogenesis, resulting in the creation of a tumor blood vessel. These vessels serve various functions, primarily by supplying nutrients and oxygen crucial for tumor growth and metabolism. Previously, it was suggested that all tumors were dependent on angiogenesis (45, 46).

Furthermore, tumor blood vessels can act as a passageway for cancer cells to metastasize to other organs. The tumor "educates" these vessels to display various phenotypic characteristics, such as the hyperactivation of Notch signaling in endothelial cells, which make the cancer cells more aggressive after extravasation and allow them to proliferate successfully at metastases (47).

In pathological angiogenesis induced by tumors, the newly formed blood vessels are known to be highly leaky due to the lack of smooth muscle cells, pericytes, and unorganized lining of basement membrane which can be advantageous for cancer cell extravasation and intravasation for metastasis (48). Consequently, the efficacy of various drugs is reduced because they cannot

penetrate deep into the tumor. By manipulating the tumor vasculature, vessel normalization can be induced, ultimately increasing the effectiveness of chemotherapy delivery (49, 50). In fact, research has shown that anti-angiogenic therapies approved for cancer treatment may induce hypoxia instead of suppressing the tumor blood supply, promoting tumor progression. Therefore, vessel normalization, rather than suppressing angiogenesis, has gained attention as an effective cancer therapy (51).

The mouse in a healthy state mainly produces immune cells and erythroid cells that are generally differentiated from HSCs in the bone marrow (52). In tumors, myeloid cells such as MDSCs are recruited through the secretion of various cytokines due to their short lifespan (53,54). Excessive myelopoiesis causes myelofibrosis of the bone marrow by monocyte-derived fibrocytes, which is the main cause of tumor-associated anemia (55,56). Due to stress such as anemia, the bone marrow loses its function, promoting extramedullary hematopoiesis (EMH) in the liver and spleen. This can result in hepatosplenomegaly, which is frequently observed in some cancer patients and murine tumor models (57).

Studies have shown that erythroid cells and myeloid cells are enriched in splenomegaly. Erythroid cells originate from HSCs and include erythrocytes and erythroblasts. Among them, $CD45^{+}$ erythroid cells infiltrate inside the tumor to express arginase, TGF-β, ROS, while $CD45^{-}CD71^{+}$ erythroid cells produce artemin in the spleen, ultimately promoting tumor progression in hepatocellular carcinoma (HCC) (58,59). Myeloid cells, such as

MDSCs, monocytes, tumor-associated macrophages (TAMs), and neutrophils, have also been reported to contribute to tumor progression and immune suppression through various pathways (60).

Based on these data, phenotypic differences between Tcon and Dcon tumors should be well-defined, so that Tcon and Dcon tumor models can represent certain subtypes of gastric cancer and therefore establish optimal therapeutic strategy. Thus, my study states phenotypic characteristics of Tcon and Dcon tumors with insights for clinical implications

Materials and Methods

Cell culture

Tcon and Dcon cell lines were cultured in DMEM (Biowest, L0103), incubated in a 37° C, 5% CO_2 incubator.

Animal models of subcutaneous tumor

Six to eight-week-old WT male C57BL/6 mice were anesthetized with ketamine (100mg/kg) and xylazine (10mg/kg) solution in PBS, with intraperitoneal injection at dosage of 200 μL/20g. Ear tags were applied for each mouse, and hair on the right flank was carefully removed with clippers. Tcon and Dcon cells were washed with 10mL of PBS twice, and detached from the culture plate with Trypsin/EDTA solution. 1 x 10^6 Tcon or Dcon cells in 100 μL of PBS were subcutaneously injected in the right flank, after disinfection with 70% ethyl alcohol. Tumor growth were monitored every 3days beginning at 7days after injection. The volume of the tumor was calculated as following; (long shaft) X (short shaft)^2/2.

Single-cell dissociation of tumors

Tcon and Dcon subcutaneous tumors were resected, chopped into small pieces ($\leq$1mm^3). Tissues were then enzymatically digested in the digestion buffer, prepared with fresh DMEM, Collagenase type VI (1mg/ml,

Sigma), DNAse type I (1.5mg/ml, Sigma), Hyaluronidase (1mg/ml, Sigma) and incubated in a 37° C, 5% CO_2 incubator for 20 min. Tissues were filtered through 70 μm cell strainers to be dissociated in to single-cell suspension. Cell numbers were estimated using hemocytometers after trypan blue staining.

Flow cytometry

$5x10^5$ of Single-cell suspension of Tcon and Dcon tumors were washed with FACS buffer (0.5% Bovine Serum Albumin, 0.1% Sodium Azide in PBS) and stained with LIVE/DEAD stain kit (Thermo, L34955) for 30 min in 4° C, dark. Cells were washed with FACS buffer and stained with surface antibody cocktail (1:200 each). Antibodies used for the staining are listed (Table 1). Cells were then fixed with Intracellular fixation buffer (invitrogen) for 30min in RT, washed with permeabilization buffer(Invitrogen) and stained with intracellular antibody cocktail (1:100 each) Foxp3 staining kit (Invitrogen) were used for staining Foxp3 to permeabilize the nuclear membrane, and cells were stained with antibody solution (1:200) Cells were then washed with 1mL of FACS buffer, and filtered through 40 μm cell strainer to prevent cell clogging. Each samples in FACS tubes were read by LSRII, and data were analyzed using Flowjo v10 software.

RNA isolation

Tissue samples such as Tcon and Dcon tumors or spleens were harvested, and chopped in 1mL of TRIzol on ice. Chopped tissues were moved in mortar, and liquid nitrogen was added to freeze the samples. Frozen

tissues were crushed promptly, and 1mL of TRIzol was added for each 20mg of tissue sample. 200μL chloroform was added and incubated for 5min in RT. Cells were centrifuged in 12000g, 4° C for 15min, and aqueous phase was collected and moved into other 1.5mL tubes. 500μL isopropyl alcohol was added and tubes were incubated for 10min in RT, after mixed vigorously. Tubes were centrifuged in 12000g, 4° C for 15min, and the pellets were washed with 70% ethanol with centrifugation in 7500g, 4° C for 5min. Pellets were completely dried from remaining ethanol, and quality of the RNA were measured with NanoDrop spectrophotometer. (1.8 < A260/A280 < 2.0, 2.0 < A260/A230 < 2.2)

qRT-PCR

To obtain cDNA, a reverse transcription reaction was carried out using the GoScriptTM reverse transcriptase kit (Promega, A5003) on high-quality RNA up to 5 μg. Amplification reactions were performed using the SYBR™ Green PCR Master Mix kit on a Real-Time PCR System (Applied Biosystems). Oligonucleotide sequences that are used for primers are listed (Table 2). The expression level was determined using the ΔΔCT method, and Gadph was used as a housekeeping gene for internal control.

RNA-seq

RNA-seq was performed by Macrogen. Briefly, samples were sequenced using an Illumina platform, Average of 74.0 million paired-end reads was sequenced across 8 RNA samples from Tcon and Dcon tumors. After Illumina universal adapters were trimmed, the reads were mapped to the Mus musculus GRCm38(mm10) reference genome using the HISAT2 to

generate the aligned reads. Known transcripts were quantified using StringTie and normalized via DESeq2. For comparison of Tcon tumors and Dcon tumors, genes with an adjusted P value of <0.05 and absolute log2 (fold change) of >1 were utilized as differentially expressed genes (DEGs). For assessment of differentially upregulated pathways in Tcon and Dcon tumors, Top 500 DEGs each with unadjusted P value of <0.0005 were plugged into https://maayanlab.cloud/Enrichr/.

Immunofluorescence

Tcon and Dcon subcutaneous tumors were resected, washed with PBS and fixed in 4% PFA for 6~12h in 4° C. Tumors were equilibrated in 30% sucrose solution overnight, and were frozen with OCT compound. Frozen blocks were carefully cryosectioned with 20μm thickness, and mounted on slides. Tumor sections were re-moisturized with 0.2% PBSTX(PBS + Triton-X), and blocked with 10% serum from the host of the secondary antibodies for 1h in RT. Primary antibodies diluted with pre-optimized concentration in 5% serum in 0.2% PBSTX were added to the slide, and tissues were incubated for overnight in 4° C. After primary antibody staining, Primary antibodies : anti-CD31 (2H8, Merck, cat# MAB1398Z), anti-αSMA-Alexa Fluor 647 (1A4/asm-1, Novus biologicals, cat# NBP2-34522AF647). the slides were washed with PBSTX thrice for 3min each, and incubated with secondary antibody solution with pre-optimized concentration. Secondary antibody : AlexaFluor647 (Invitrogen, cat# A-21451) After washing thrice with PBSTX, slides were added with a drop of Vectashield Mounting Medium containing DAPI (Vector Laboratories), and covered with coverslip. IF slides were visualized using FV3000 confocal laser scanning microscope.

Perfusion assay

Mice were anesthetized by intraperitoneal injection of Ketamine-xylazine solution of 200μL/20g, and then intravenously injected into the retro-orbital space with 100ul of 2000kDa TRITC-Dextran (TdB Labs, TD2000; 20mg/kg) or PBS as negative control, and were sacrificed 15min after the injection. Tcon and Dcon tumors were fixed in 4% paraformaldehyde for 6 hours at 4° C and equilibrated in 30% sucrose overnight at 4° C. The tumors were then embedded in O.C.T. compound (TissueTek), and 20-μm-thick cryosections were prepared. The sections were blocked with 10% goat serum in PBST (0.4% Triton X-100) for 1 hour and stained with the AlexaFluor647-conjugated secondary antibodies following anti-CD31 antibody to analyze positive signal area.

Collagen imaging using SHG

Mice bearing Tcon and Dcon tumors were anesthetized and incisions were made on skin adjacent to the tumor with sterilized forceps and tweezers. Skin was flipped upside-down to expose the tumor, and fixed with forceps or needles. The exposed tumors were cleansed with sterilized DW to wash contaminants, particles or furs, and mice were moved to the microscope (IVM), and rectal probe for body temperature monitoring was inserted. Two-photon microscopy Second Harmonic Generation (SHG) imaging was proceeded with wavelength of 840nm to visualize intratumoral collagen fiber, and laser power between 5% to 25%. The incision on the skin of mice were carefully disinfected with 70% ethanol applied on sterile gauze, and sutured after the imaging. Z-stack images were produced with

optimized numbers of slices or intervals, and averaged in maximum intensity with IVM studio software. The processed images were quantified with collagen fibers by ImageJ software.

Hemoglobin measurement

4 μL of blood from WT mice, Tcon or Dcon tumor bearing mice were harvested and mixed with 996 μL of Drabkin's reagent in 1.5mL microtube. The microtubes were agitated for 15min in RT, and OD in 540nm were measured using Nanodrop spectrophotometer.

RESULTS

E-Cadherin was knocked out in Tcon cell while expressed in Dcon cell

Before generating Tcon and Dcon tumor models via subcutaneous injection on C57BL/6 mice, I urged to verify that Tcon cell lacks Cdh1 gene expression, which encodes E-Cadherin. To begin with, I performed PCR with primers that target exon 7 of murine Cdh1 gene, which is flanked in $Cdh1^{fl/fl}$ mouse that was used to generate Tcon mice in Till et al. (Fig 1A). Through gel electrophoresis of PCR-amplified DNA samples extracted from Tcon and Dcon cell; Tcon : Atp4b-Cre; $Rosa26^{LSL-YFP}$; $Trp53^{fl/fl}$; $KrasLSL^{G12D/+}$; $Cdh1^{fl/fl}$, Dcon : Atp4b-Cre; $Rosa26^{LSL-YFP}$; $Trp53^{fl/fl}$; $KrasLSL^{G12D/+}$; $Cdh1^{fl/+}$, I could verify that Tcon cells lack Cdh1 gene in their gDNA (Fig 1B). Furthermore, I performed qRT-PCR of mRNA extracted from Tcon and Dcon cells to measure Cdh1 expression (Fig 1C). The C_T values of Cdh1 gene were undetermined in Tcon cells, thus no Cdh1 transcript was detected. On the other hand, C_T values of Cdh1 gene from Dcon cells were 36.41 in average(n=3), which was quite high compared to C_T values of Gapdh, implying that Cdh1 gene in Dcon cells are transcribed into mRNA, reflecting their heterozygous

origin.

Tcon and Dcon tumors display distinct phenotypic characteristics

Subcutaneously injected Tcon and Dcon tumors were examined for apparent characteristics and patterns of tumorigenicity and tumor growth. Injected Tcon cells became distinguishable tumors at Day 7, and showed slow tumor growth. Dcon tumors were detected at Day10~13, however, showed fast tumor growth (Fig 2A-B). While Tcon and Dcon tumors had similar volume and weight at 27 days after injection, Tcon tumors displayed the tendency of paleness and overall stiffness and Dcon tumors tend to be red, due to vascularization and internal bleeding (Fig 2C-D). Interestingly, spleens of Dcon tumor-bearing mice were enlarged compared to Tcon tumor-bearing mice or WT mice, which impose that Dcon tumors might possess potentials to systematically affect the tumor macro-environment (Fig 2E-F).

Tcon tumors are highly enriched with αSMA^{+}PDPN^{-}PDGFRA^{-} CAF, a potential key regulator of desmoplastic reaction in Tcon tumors.

Since the composition of TME tend to be largely affected by the size of the tumor, I set time point of analysis at 25~28 days after injection, when size of two types of tumors become similar for accurate and unbiased analysis between Tcon and Dcon tumor and

properly exclude the effects of tumor size.

Excessive deposition of extracellular matrix (ECM) including collagen fiber is known to be one of the major cause of desmoplastic tumors which confers stiffness and rigidity to tumor mass. The desmoplastic tumors are also found in scirrhous gastric adenocarcinoma, usually accompany linitis plastica, and spontaneous Tcon tumors reported in Till et al. I observed collagen fibers in Tcon and Dcon tumors with Second Harmonic Generation (SHG) imaging and produced averaged Z-stack images (Fig 3A). Average collagen-positive area per Region of Interest (ROI) was significantly high in Tcon tumors (Fig 3B).

CAFs are known to be one of the crucial factors for tumor progression undergoing various biological pathways including desmoplastic reaction that disrupts delivery of therapeutic agents. Sine CAFs are also one of the main sources of ECM production, including collagen fibers, I sought to define the protein markers of CAFs in order to measure the populations CAFs and several subtypes. I adopted 3 protein markers of CAFs, αSMA, PDPN and PDGFRα which were well-defined in previous researches on PDAC, one of aggressive cancers due to its severe desmoplasia. I performed multi-channel flow cytometry analysis on Tcon and Dcon tumors to quantify overall CAF population and subsets. CAFs were gated upon non-immune, non-endothelial, stromal cells (Non-debris / singlet / live / YFP^- / $CD45^-$ / $PECAM^-$ / $EpCAM^-$)

and were defined as non-immune stromal cells that express at least one of the markers among αSMA or PDPN or PDGFRα (Fig 4A). Furthermore, I examined the expression of Ly6C and I-A/I-E to classify myCAFs ($Ly6C^{-}I-A/I-E^{-}$), iCAFs ($Ly6C^{+}I-A/I-E^{-}$), apCAFs ($Ly6C^{-}I-A/I-E^{+}$) which are well-defined CAF subsets in Elyada et al., each of which represents myofibroblastic CAFs that are responsible for fibrosis and ECM production, inflammatory CAFs that secretes cytokines that promotes immune suppression of the tumor, and antigen presenting CAFs that are supposed to activate regulatory T cells to confer immune suppressive condition to the tumor (Fig 4B). Moreover, I measured PD-L1 expression of CAFs, since there are several reports that CAFs can also abrogate $CD8^{+}$T cells' anti-tumoral function by expressing PD-L1, a well-known immune checkpoint ligand (Fig 4C).

Total CAFs that express at least one marker among αSMA, PDPN, PDGFRα existed in substantial size of population in Tcon tumor (Fig 5A). Moreover, αSMA single-positive CAFs showed large population in Tcon tumor with αSMA^{+}CAFs, including αSMA single-positive CAFs, were also highly populated in Tcon tumors (Fig. 5B). myCAFs were also enriched in Tcon than Dcon tumors (Fig 5C), which is consistent with the findings that Tcon tumors are more fibrotic and more enriched with αSMA single-positive CAFs that are hypothetically induce desmoplasia in Tcon tumors. Furthermore, apCAFs, with their relatively small population, are also enriched in Tcon tumors that might contribute

immunosuppressive TME (Fig 5C).

Additionally, there have been several reports on CAF subsets that express PD-L1 exert immunosuppression on TME in certain cancer types (61,62). I measured the expression of PD-L1 of CAFs in Tcon and observed high PD-L1 expression on CAFs (Fig 5D). Therefore, I could confirm that not only CAFs that induce severe desmoplasia, but also CAFs that express immune checkpoint ligand molecules are enriched in Tcon TME.

To verify that Tcon tumors are enriched with αSMA^{+}CAFs, I performed immunofluorescence staining of Tcon and Dcon tumor sections with anti-αSMA antibody. As a result, Tcon tumors showed significantly high ratio of αSMA localization (Fig 6A-B). Also, I measured the expression of Acta2, which encodes αSMA in RNA samples extracted from Tcon tumors, which was 3.47 fold higher in Tcon tumors (Fig 6C). Tgfb1, which encodes TGF-β1, a key regulator of fibroblast activation, transition to myofibroblast and most importantly, differentiation into myCAFs (21) was also upregulated in Tcon tumors, thus, confirmed that myofibroblast-like CAFs (αSMA^{+}CAFs or myCAFs) were highly enriched in Tcon tumors (Fig 6D).

I also analyzed RNA-sequencing data of Tcon and Dcon cell culture to figure out tumor cell-derived factors that could recruit and activate CAFs. Interestingly, Wnt7a gene, one of ligands of

Wnt/β-catenin pathway was exclusively expressed in Tcon cells (Fig 6E). Wnt7a was reported to activate CAFs into myofibroblastic state in mouse mammary carcinoma including 4T1 and 410.4 orthotopic tumors (67). Thus, it can be hypothesized that Wnt7a secreted from Tcon cells might have activated normal fibroblast recruited into the Tcon tumor stroma to CAFs that induce desmoplastic reaction.

In summary, I verified that certain CAF subtypes, such as αSMA single-positive CAFs, or myCAFs consists higher portion of TME, which may be a direct cause for desmoplasia and discovered potential CAF-activating factor, Wnt7a in Tcon tumors.

Tcon tumors are poorly vascularized with low functionality in terms of blood perfusion

Unlike Tcon tumors that are pale in color, Dcon tumors tend to be blood-red, and contain hemorrhagic region inside the tumor (Fig 2C). I performed immunofluorescence staining on Tcon and Dcon tumor sections with anti-CD31 antibody to quantify the tumor blood vessels (Fig 7A). As a result, Dcon tumors showed substantial $CD31^{+}$area, implying large population of endothelial cells (Fig 7B). Since the value of $CD31^{+}$area/ROI represents the circumference of the blood vessels, I sought to measure the area of the blood vessels too (Fig 7C). Total area of blood vessels and average area of each blood vessels in ROI were found to be low in Dcon tumors (Fig 7D-

E). Therefore, I could verify that overall vascularization was highly deficient and repressed in Tcon tumors in several aspects.

Tumor blood vessels, however, generally display distinct phenotypes from their normal counterparts, owing to various interactions and signals inside the TME. One of the characteristics is lack or deficiency of coverage by pericytes which lead to leakage of the vessel and ultimately leave the blood vessel without the perfusion. Therefore, pathologic angiogenesis can produce mal-functional blood vessels. I urged to verify that Tcon tumors are not only poorly-vascularized, but also possess low functionalities of blood vessels. There are several methods to measure the blood vessel functionality, such as immunofluorescence with NG2, a pericyte marker, however, the most direct and precise parameter for blood vessel functionality is blood perfusion. 2000kDA TRITC-dextran was i.v. injected into the Tcon and Dcon bearing mice, and performed immunofluorescence using anti-CD31 antibody (Fig 8A). The IF images from Tcon and Dcon tumors with 2000kDA TRITC-dextran injection show that TRITC-dextran^{+}area / CD31^{+}area was significantly low in Tcon tumors (Fig 8B). In addition, CD31^{+}area was also low in Tcon tumors, thus, I could double-check that vascularity in Tcon tumors were deficient in two different experimental sets (Fig 7B, Fig 8C).

To be noted, according to the RNA-seq data of Tcon and Dcon tumors, I was able to find out that Tcon tumors have high

expression of Angpt2, and low expression of Angpt1. Angpt2 is a well-known angiogenic factor, however, also function as destabilizing blood vessels by detaching pericytes, thus, the vessels show low blood perfusion and leaky characteristics. On the other hand, Angpt1, which is also an angiogenic factor, however, antagonize Angpt2, therefore stabilize the blood vessels. It has been also reported that high Angpt2 : Angpt1 ratio is correlated to poor prognosis in several types of cancers (63).

In comprehensive view, these data suggest that Dcon tumors have undergone active angiogenesis, while Tcon tumor haven't, supposedly because of the vessel compression by severe desmoplastic reaction with excessive ECM accumulation that applies physical pressure to the blood vessels. Thus, while chemo therapy or immune therapy on Tcon tumors might not exhibit good responses due to repressed drug delivery, Tcon tumors might display low therapy responses.

Dcon tumors displayed high immune cell infiltration with substantial portion of effector T cells

I performed multi-panel / multi-channel flow cytometry analysis for overall immune cell profiling, which are the major components of the TME. Based on cell markers (table 3-4) and gating strategy (Fig 9, Fig 10). Lymphoid cells including T cells, B cells and NK cells and myeloid cells including MDSCs, monocytes, macrophages,

DCs and neutrophils were analyzed. To begin with, total immune cell population ($CD45^+$) was significantly high in Dcon tumors (Fig 11A). Most of the immune cell populations including $CD4^+$T cells, $CD8^+$T cells, B cells, NK cells, M-MDSCs, Classical monocyte(CM)s, $CD11c^+$DCs, Macrophages, M1-like and M2-like types were significantly enriched in Dcon tumors (Fig 11B-G, cell populations without statistical significance not shown). Furthermore, macrophages, and M1-like, M2-like subtypes per total live cells in Dcon tumors showed large populations, however, M2-like macrophages per total macrophages was low, while M1-like macrophages per total macrophages was high in Dcon tumors (Fig 11H-I). Since M2-like subtypes of macrophages are known to exert immunosuppressive effects on several types of tumors, it could be suggested that even with lower absolute number of M2-like macrophages, Tcon tumors might possess potentials to form immunosuppressive TME, along with the suppressive function of PD-$L1^+$CAFs (Fig 5D).

Moreover, I measured effector T cells, which are known to secrete various cytokines including TNFα, Interferon-γ, Granzyme B, Perforin in Tcon and Dcon tumors through flow cytometry to verify that Dcon tumors not only display substantial population size of $CD4^+$T cell and $CD8^+$T cell, but also high percentage of anti-tumoral effector T cells. The single-cell suspension prepared from Tcon and Dcon tumors were stimulated for 4h in PMA + ionomycin cell activation cocktail with Brefeldin A and stained with antibodies

that targets the indicated antigens. Based on the flow cytometry gating strategy for cytokine panel (Fig 12), Tcon and Dcon tumors were analyzed with their effector T cells in the TME. In case of $CD4^+$T cells, TNFα, GranzymeB, Perforin, Interferon-γ positive cell populations were significantly high in Dcon tumors (Fig 13A-D). Also, $CD8^+$T cell populations that express each of TNFα, Granzyme B, Perforin, Interferon-γ were also high in Dcon tumors than in Tcon tumors (Fig 13E-H). In summary, Dcon tumors showed large immune cell populations, probably owing to extensive angiogenesis of vessels with high blood perfusion, so that immune cells from blood and lymphoid organs easily infiltrate into the tumor. Furthermore, T cells with effector functions, defined as ability to produce and secrete several cytokines including TNFα, Granzyme B, Perforin, Interferon-γ compared to total T cells were high in Dcon tumors, possibly due to higher proportion of M1-like macrophages than M2-like macrophages.

Dcon tumor bearing mice displayed severe splenomegaly, enriched with myeloid cells and erythroblasts.

Spleen is one of the most important secondary lymphoid organs, in which homing of various immune cells proceeds, so that it can function as major site of immune response. Spleen is also known to affect tumor progression, since not only can it act as a reservoir for immune cells that infiltrate into the tumor, but also drives elevated myelopoiesis in hosts of several cancer types to generate myeloid cell that might possess pro-tumoral functions. Spleens resected from the mice 27 days after injecting Dcon cell were enlarged, which indicate splenomegaly (Fig 2D). Unlike the general idea that advanced tumors can induce splenomegaly, Tcon tumor bearing mice that had larger tumors than Dcon tumor bearing mice did not showed splenomegaly, which impose that occurrence of splenomegaly is more relevant to cancer type than it is to the tumor size (Fig 14A). Splenomegaly is known to be induced by stress signals from tumor-associated anemia. Anemia promotes HSCs to migrate into secondary hematopoietic organs such as spleen and liver, and proceeds EMH within. However, aberrant hematopoiesis can abnormally produce certain cell types, and ultimately enlarges the organ, which is termed as hepatosplenomegaly. To verify the process that induces splenomegaly, I firstly measured hemoglobin level in Tcon and Dcon tumor bearing mice, and WT mice using Drabkin' s reagent. As a result, Dcon tumor bearing mice showed about 50% of hemoglobin level compared to WT mice, which

confirmed severe anemia in Dcon tumor bearing mice, even in relatively earlier time point (Fig 14B). Then, I tried to verify the cell types that are enriched in the spleen with splenomegaly and performed flow cytometry analysis on lymphoid cells and myeloid cells. As a result, $CD45^{+}CD11b^{+}$ population, including myeloid cells and MDSCs were enriched, while, $CD45^{-}$ population was also enriched in the enlarged Dcon tumor bearing mice (Fig 14C). Among the various myeloid subsets, PMN-MDSCs, neutrophils, M-MDSCs, and CMs have undergone extensive proliferation, of which were also enriched in Dcon tumors, ultimately explains that certain myeloid subsets were generated through severe myelopoiesis accompanied by splenomegaly, and infiltrated into the Dcon tumors (Fig 11E-F, Fig 14D-G). On the other hand, in case of $CD45^{-}$ population, most of them expressed TER-119, a well-known erythroid lineage marker protein. However, for accurate measurement and analysis, I lysed the erythrocytes by RBC lysis buffer during the flow cytometry sample preparation, and also excluded erythrocytes through FSC-A/SSC-A gating, thus, TER-119 expressed on erythrocytes could not have been estimated. Therefore, I hypothesized that the enriched cells were precursor cells of erythrocytes that are not enucleated so that they can remain after the RBC lysis procedures. Erythroid precursor cells are known to express CD71, an erythroid precursor marker protein, of which shows higher expression when the cell is less differentiated. Erythroblasts are the least differentiated cells in erythroid lineage that also express high degree of CD71 protein.

Most of the $CD45^{-}TER-119^{+}$ cells in the spleens of Dcon tumor bearing mice also expressed CD71, which indicates the enrichment of splenic erythroblast in Dcon tumor bearing mice (Fig 14H-I). In addition, "Ter-cells", termed after TER-119 expression were reported to be expanded in the enlarged spleen of HCC patients and HCC murine model, share the same protein marker with my results. However, while Ter-cells secrete artemin, a neurotrophic factor, which promotes tumor growth, erythroblasts verified in the spleen of Dcon tumor bearing mice did not (Data not shown)(58). In summary, I was able to verify major cell types that were enriched in the Dcon tumor bearing mice's spleen with splenomegaly, which are myeloid subsets and erythroblasts. However, the mechanism how the erythroblasts affect the tumor progression should be verified for further studies.

RNA-sequencing of Tcon and Dcon tumors reveal differential enrichment of biological pathways.

For unbiased screening of DEGs (Differentially expressed genes) between Tcon and Dcon tumors, I analyzed RNA-seq data of RNA extracted from Tcon and Dcon tumor samples. Raw data were processed and normalized via DESeq2 and genes that showed absolute log2FoldChange higher than 1, and adjusted P value lower than 0.05 were regarded as DEGs. Then, top 500 DEGs from each tumor type were applied for pathway enrichment analysis via Enrichr (Fig 15A-B) (64). Tcon tumors were enriched with Foxa2 pathway, and EMT in CRC in Wikipathway 2021 human dataset, and Tight junction interaction, Hnf3b

pathway in BioPlanet 2019 dataset. Foxa2 pathway including Foxa2 and Gsta1 are known to enhance the invasive ability and proliferation while reduced apoptosis of human colon cancer, esophageal squamous cell carcinoma, lung cancer (65-68). Furthermore, Wnt4, considered as a major component of EMT pathway in CRC was also upregulated in Tcon tumors. Interestingly, Wnt4 not only contributed to EMT, but also induced pathologic angiogenesis via Wnt4/Ang2 pathway, which is consistent with the previous data that Tcon tumors have higher ratio of Angpt2 : Angpt1 which indicates mal-functional blood vessels (Fig 8D).

Tcon tumors also displayed elevated expression of claudin family genes that compose tight junction interaction pathway and cell junction organization pathway. Claudin genes including Cldn6 and Cldn4 are well-known to encode tight junction proteins, however, their function in several types of solid tumors have also been reported. Especially, Cldn6 promoted invasive and proliferative abilities of gastric cancer cell via YAP1-snail1 axis (69-71).

On the other hand, Dcon tumors displayed quite different enrichment of biological pathways, including heme metabolism and IFNγ/IFNα response in MSigDB Hallmark 2020, T cell activation, CTL activity, and immunoregulatory interaction in BioPlanet 2019. Markers of erythroid cells through erythroblast to erythrocyte, such as Gypa, Gypc, Ermap were detected. Moreover, genes related to heme synthesis were also detected in bulk-seq data, suggest that not only erythrocyte, which might be enriched in Dcon tumors due to higher vascularity, erythroid precursor cells including erythroblasts that are capable of producing hemoglobin also exist in Dcon tumors. Several literacies state that intratumoral erythroid cells can exert pro-tumoral / immunosuppressive function in tumor (72-74). Moreover, Dcon tumors also enriched with interferon response-

related genes. IFNγ exerts anti-tumoral effects including M2-like to M1-like polarization, Dendritic cell activation, effector T cell activation, and inhibition of T_{reg}s. IFNγ also induce cancer cell apoptosis, tumor dormancy and tumor senescence through several pathways and in the same time, enhance ICB efficacy (75). Meanwhile, it has been reported that Type 1 interferon, including IFNα also suppress tumor growth by activating STAT3-GZMB pathway in CTLs (76). However, previous research on IFNα and IFNγ states that IFNα and IFNγ could induce expression of PD-L1, encoded by Cd274, via JAK-STAT signaling. Thus, Dcon tumors are upregulated with interferon response-related genes, however, despite well-known anti-tumoral functions of interferons, immunoregulatory effects could also be exerted on tumors (77).

According to BioPlanet 2019 database, Dcon tumors were assigned to have enhanced expression of gene sets, mainly related to T cell activation and immunoregulation. Dcon tumors showed high expression of genes related to co-stimulation of T cell such as CD28 and CD80, and also cytotoxic cytokine such as GZMB. However, Dcon tumors also showed higher expression of genes related to immune-regulatory interactions, including CD96 that is known to regulate cytotoxic activity of NK cells and CD8+T cells as immune checkpoint molecule (78).

Table 1. List of antibodies used in flow cytometry

Target Antigen	Clone	Conjugation	Vendor	Cat#
CD3	17A2	BUV395	BD	740268
TER-119	TER-119	BV421	Biolegend	116234
Ly6C	HK1.4	BV510	Biolegend	128033
CD4	RM4-5	BV510	Biolegend	100559
I-A/I-E	M5/114.15.2	BV605	Biolegend	107639
CD19	6D5	BV605	Biolegend	115540
B220	RA3-6B2	BV605	Biolegend	103244
CD11c	N418	BV650	Biolegend	117339
TNF-α	Mp6-xt22	BV711	Biolegend	506349
CD31	390	BV711	Biolegend	102449
CD11b	M1/70	BV711	Biolegend	101242
CD71	C2(RUO)	FITC	BD	553266
CD8a	53-6.7	PE	Biolegend	100708
PDGFRα	APA5	PE	Biolegend	135906
Granzyme B	NGZB	eFlour610	invitrogen	61-8898-82
CD86	GL-1	PE/Dazzle	Biolegend	105042
CD19	6D5	PE/Dazzle	Biolegend	115554
Foxp3	FJK-16S	PE-Cy7	eBiosciences	25577382
F4/80	BM8	PE-Cy7	Biolegend	123114
CD141	LS17-9	PE-Cy7	invitrogen	25-1411-82
αSMA	1A4/asm-1	Alexafluor647	Novus bio	NBP2-34522AF647
Perforin	S16009A	APC	Biolegend	154304
Ly6G	1A8	APC	Biolegend	127614
I-A/I-E	M5/114.15.2	Alexafluor700	Biolegend	107622
EpCAM	G8.8	Alexafluor700	invitrogen	56-5791-82
NK1.1	PK136	APC/Cy7	Biolegend	108724
CD3	17A2	APC/Cy7	Biolegend	100222
CD49b	DX5	APC/Cy7	Biolegend	108919
CD19	6D5	APC/Cy7	Biolegend	115530
B220	RA3-6B2	APC/Cy7	Biolegend	103224
CD90.2	53-2.1	APC/Fire750	Biolegend	140326
TER-119	TER-119	APC/Fire750	Biolegend	116250
IFN-γ	XMG1.2	APC/H7	Biolegend	505850

Table 2. Nucleotide sequences of primers used in this study.

Target gene		Sequence (5' – 3')
Cdh1	Forward	GAC GTG GTA GAC GTG AAT GAA
	Reverse	GTG TCC CTC CAA ATC CGA TAC
Cdh1 for genotyping	Forward	AGT TCC CTG ACC ATG GCT CGT T
	Reverse	GGC TGT TGT GCT CAA GCC TTC A
Gapdh	Forward	GGG TGT GAA CCA CGA GAA ATA
	Reverse	GTC ATG AGC CCT TCC ACA AT
Tgfb1	Forward	CTC CCG TGG CTT CTA GTG C
	Reverse	GCC TTA GTT TGG ACA GGA TCT G
Acta2	Forward	TGC TGA CAG AGG CAC CAC TGA A
	Reverse	CAG TTG TAC GTC CAG AGG CAT AG
Col1a1	Forward	CCT CAG GGT ATT GCT GGA CAA C
	Reverse	CAG AAG GAC CTT GTT TGC CAG G
Artn	Forward	CTG CAC ATT ACC GCC TAC CT
	Reverse	GGG AAT GGC TGA TAC CAA AA
Angpt1	Forward	AGT TCA CCT GCC CAT TTC
	Reverse	GAG TCT TTA GGC ACC TTC TAC
Angpt2	Forward	GGG AGA AGA GAA GAG AAG AGA
	Reverse	GCT GTG CCG TGT GAA TAA
Il10	Forward	CTA TGC TGC CTG CTC TTA CTG
	Reverse	GGG AAG TGG GTG CAG TTA TT
Vegfa	Forward	GTC TGT GCT CTG GGA TTT G
	Reverse	CCT CTT TCG TCT GCT GAT TT

Table 3. Markers and gating strategy for flow cytometry of CAF panel

Cell type	Gating strategy
Cancer cells (Tcon, Dcon)	Live/YFP^{+}
Endothelial cells	Live/YFP^{-}/CD45^{-}/CD31^{+}
Epithelial cells	Live/YFP^{-}/CD45^{-}/CD31^{-}/CD326^{+}
CAFs	Live/YFP^{-}/CD45^{-}/CD31^{-}/CD326^{-}/αSMA^{+} or PDPN^{+} or PDGFRα^{+}
myCAFs	CAFs/Ly6C^{-} I-A/I-E^{-}
iCAFs	CAFs/Ly6C^{+} I-A/I-E^{-}
apCAFs	CAFs/Ly6C^{-} I-A/I-E^{+}
PD-L1^{+}CAFs	CAFs/PD-L1^{+}

Table 4. Markers and gating strategy for flow cytometry of lymphoid panel and myeloid panel

Cell type	Gating strategy
Cancer cells (Tcon, Dcon)	Live/YFP^{+}
Immune cells	Live/YFP^{-}/CD45^{+}
Myeloid cells	Immune cells/CD11b^{+}/lineage^{-} (TER−119, CD3, NK1.1, CD19, B220, Thy1.1)
PMN−MDSCs	Immune cells/CD11b^{+}/Ly6C^{+}Ly6G^{+}
M−MDSCs	Immune cells/CD11b^{+}/Ly6C^{high} Ly6G^{-}
Macrophages	Myeloid cells/F4/80^{+}
M1	Macrophages/CD86^{+}
M2	Macrophages/CD206^{+}
CD11c^{+}DCs	Myeloid cells/F4/80^{-}/CD11c^{+}I−A/I−E^{high}
Neutrophils	Myeloid cells/F4/80^{-}/non−DC/Ly6C^{+}Ly6G^{+}
Classical monocytes	Myeloid cells/F4/80^{-}/non−DC/Ly6C^{high} Ly6G^{-}
Non−classical monocytes	Myeloid cells/F4/80^{-}/non−DC/Ly6C^{low} Ly6G^{-}
Lymphoid cells	Immune cells/CD11b^{-}
T cells	Lymphoid cells/CD3^{+}
CD4^{+}T cells	Lymphoid cells/CD3^{+}/CD4^{+}
CD8^{+}T cells	Lymphoid cells/CD3^{+}/CD8^{+}
T_{reg}s	Lymphoid cells/CD3^{+}/CD4^{+}/CD25^{+}Foxp3^{+}
B cells	Lymphoid cells/CD3^{-}/B220^{+}CD19^{+}
NK cells	Lymphoid cells/CD3^{-}/non−B cells/CD49b^{+}

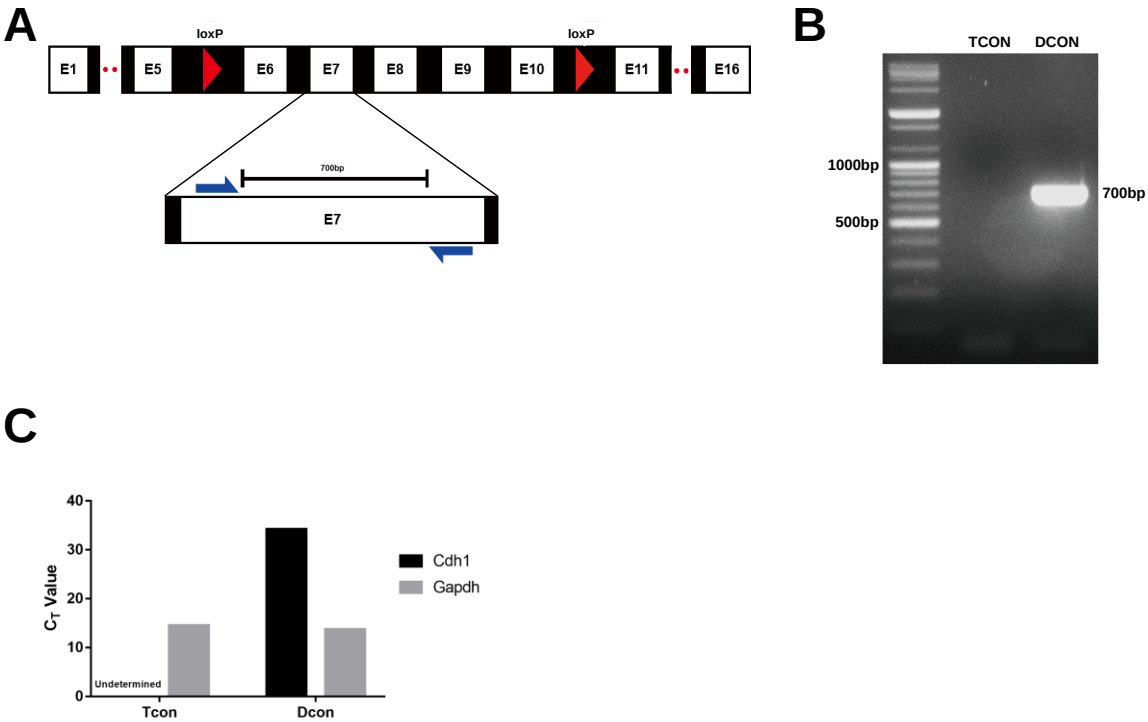

Figure 1. Differential mutation states of E-Cadherin between Tcon and Dcon cells were verified.

(A) Schematic illustration of Cdh1-flox TG mice used to generate Tcon and Dcon mice and targeting site of exon7 for genotyping. (B) gDNA extracted from Tcon and Dcon cells were amplified through PCR and gel-electrophoresis was proceeded after being loaded to 2% agarose gel. (C) C_T values of Gapdh and Cdh1 gene of Tcon and Dcon cell culture (n=3).

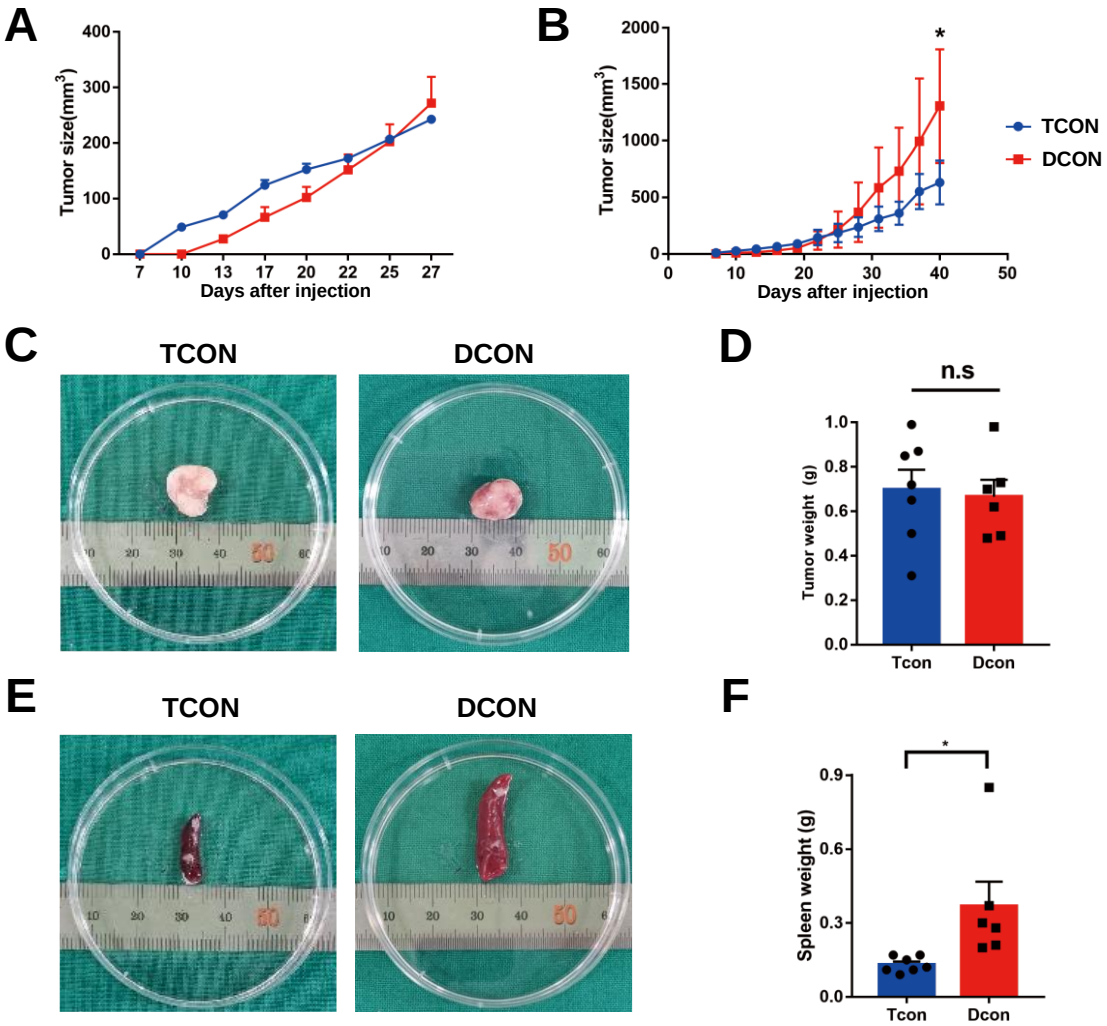

Figure 2. Tcon and Dcon subcutaneous tumors display different phenotypes. Tumor size of Tcon and Dcon subcutaneous tumors until (A) early time point (day 27) (n=7), and (B) late time point (day 40) (n=7). Gross image of (C) Tcon and Dcon tumor and (E) spleen of Tcon and Dcon tumor bearing mice after resection. Bar plots of the weight of (D) Tcon and Dcon tumors and (F) spleens of Tcon and Dcon tumor bearing mice. Data are presented as the mean ± SEM. Unpaired t-test, $^{*}P < 0.05$

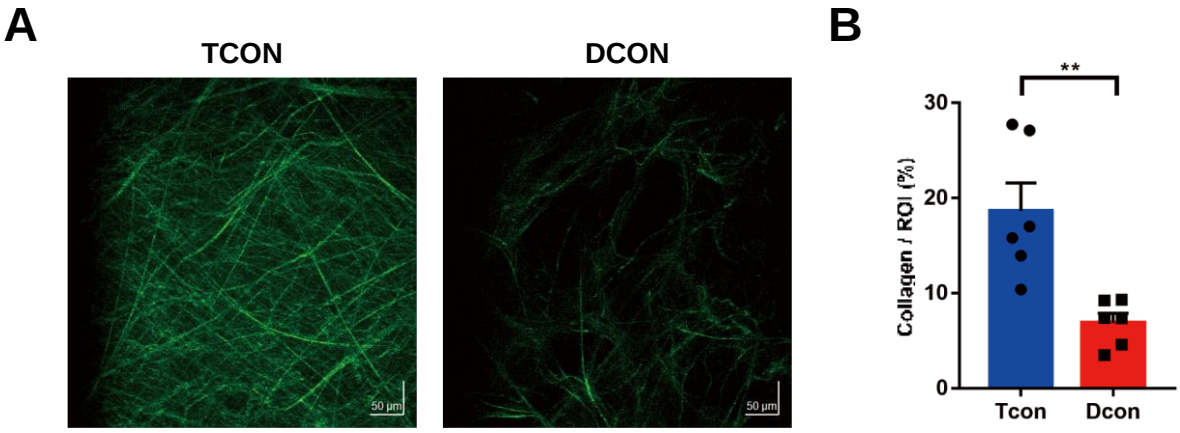

Figure 3. Tcon tumors are desmoplastic due to aberrant production of collagen fibers.

(A) Representative images of second-harmonic generation (SHG) imaging with size of 512 μm each in width and height, of which green pseudo-colored area represents the distribution of collagen fibers in Tcon and Dcon tumors. Wavelength for SHG imaging was 840nm and 20 Z-stack images were averaged into an image. (B) Average value of collagen-positive area per ROI in Tcon and Dcon tumors (n=6). Data are presented as mean ± SEM. Unpaired t-test, $^{*}P < 0.05$, $^{**}P < 0.01$

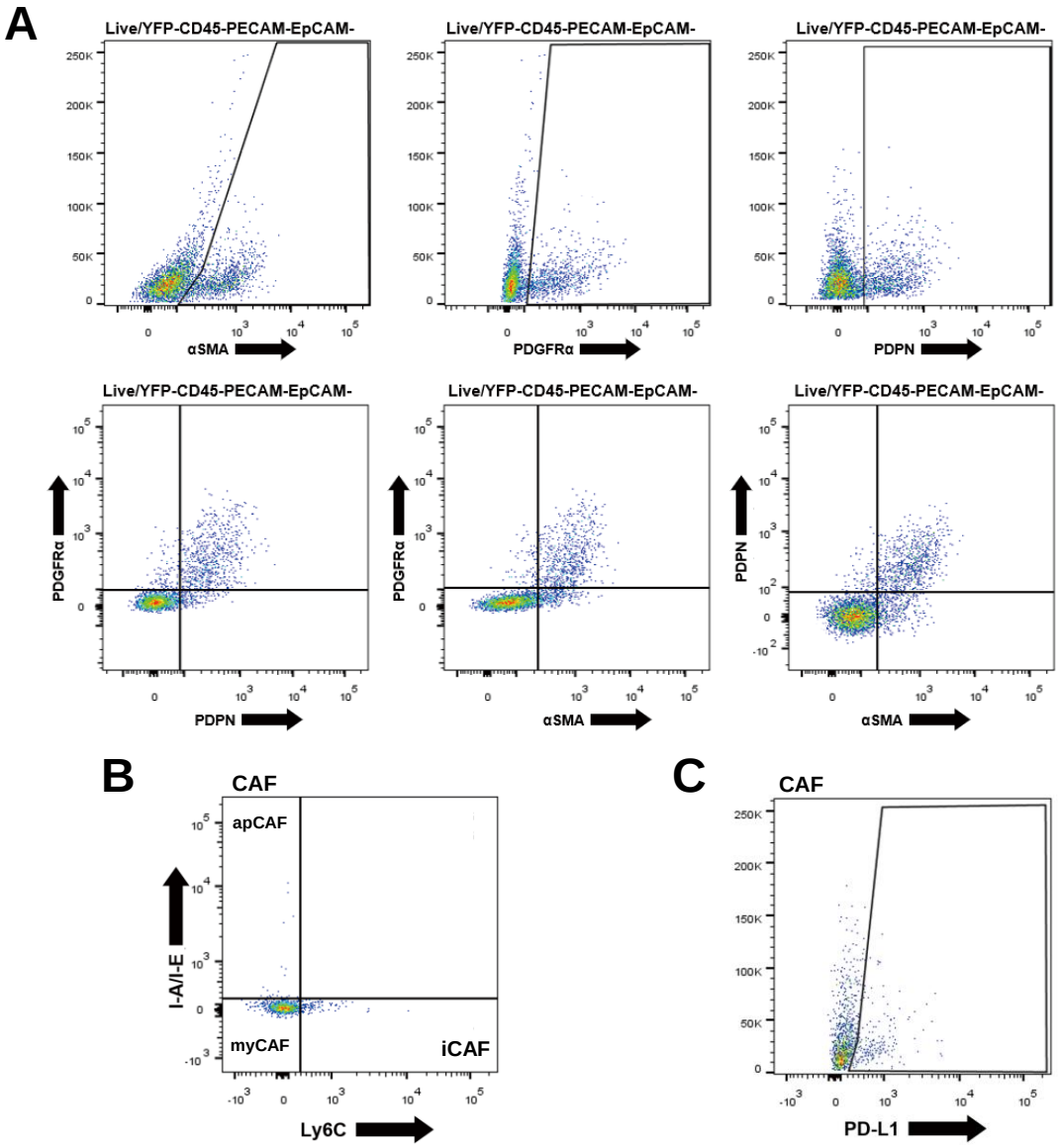

Figure 4. Expression of marker proteins of CAF and subtypes.

(A) Representative flow cytometry dot plots for CAFs that express at least one protein marker among αSMA, PDPN and PDGFRα (up), CAFs that express more than one markers among the stated proteins (down). Representative flow cytometry dot plots for CAF subsets that express (B) PD-L1, (C) myCAFs, iCAFs and myCAFs in Elyada et al.

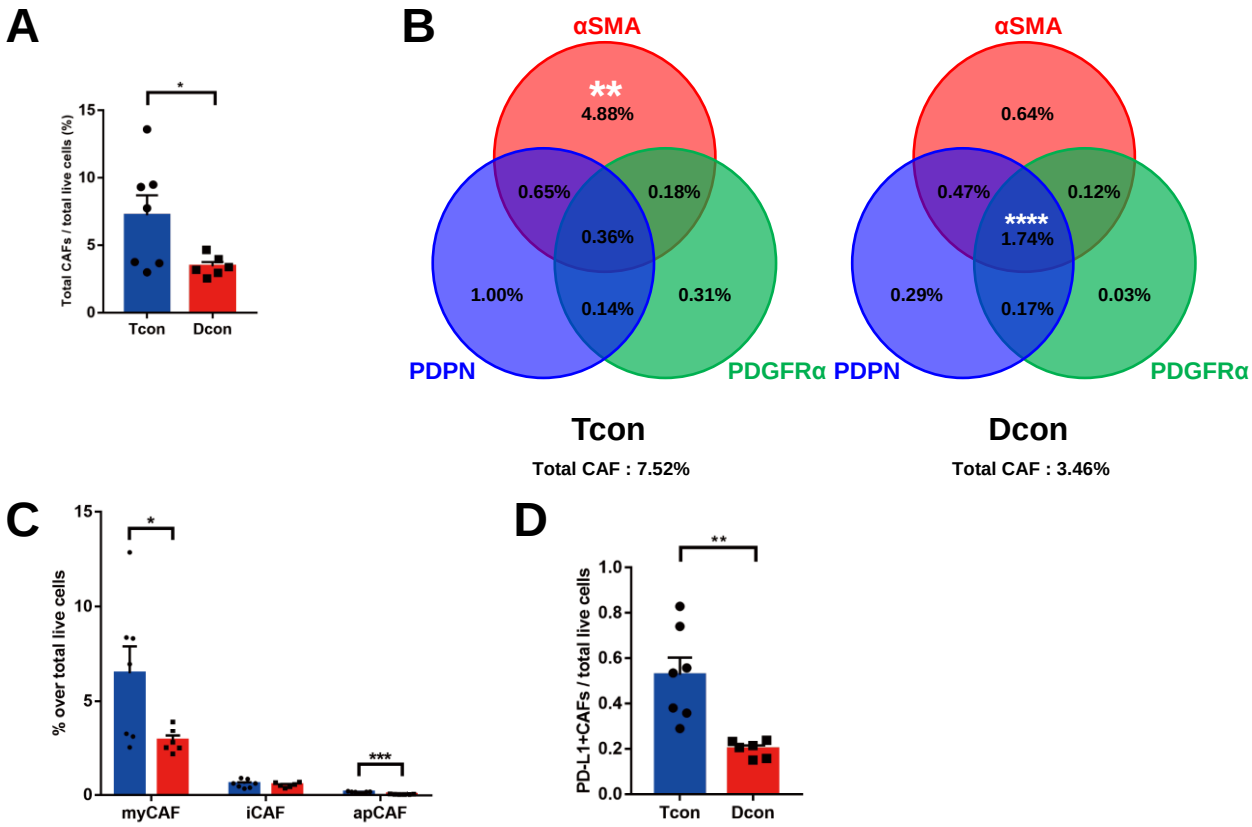

Figure 5. Tcon tumors are highly enriched with αSMA^{+}PDPN^{-}PDGFRα^{-} CAF, a potential key regulator of desmoplastic reaction in Tcon tumors.

(A) Bar plot showing the total CAF population per total live cells, which express at least one protein marker among αSMA, PDPN and PDGFRα in Tcon and Dcon tumors (Tcon : n=7, Dcon : n=6). (B) Venn diagram of CAFs classified by expression of the stated 3 protein markers. White significance symbols represent significantly higher population, compared to the same CAF subset in their counterpart (Tcon : n=7, Dcon : n=6). Bar plots showing (C) myCAFs, iCAFs, apCAFs and (D) PD-L1^{+}CAFs per total live cells in Tcon and Dcon tumors measured via flow cytometry analysis (Tcon : n=7, Dcon : n=6). All data are presented as mean ± SEM. Unpaired t-test, $^{*}P < 0.05$, $^{**}P < 0.01$, $^{****}P < 0.0001$.

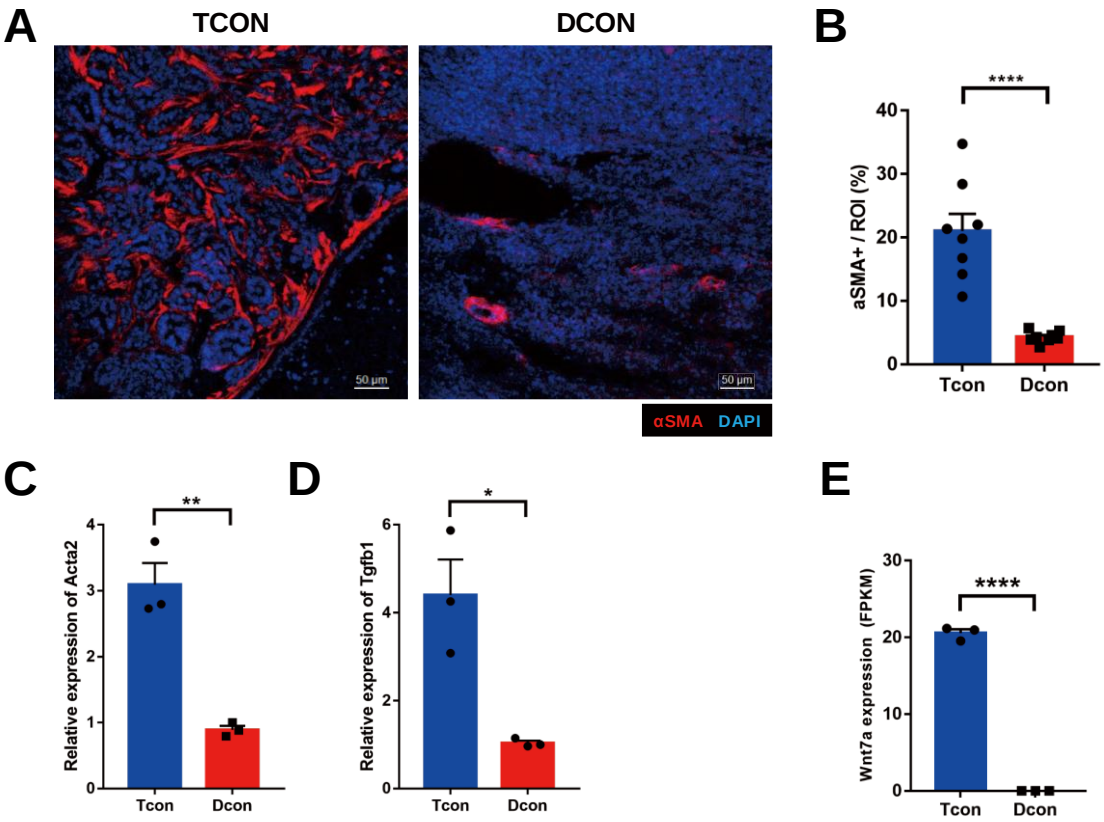

Figure 6. αSMA^{+}CAF is a potential key regulator of desmoplastic reaction in Tcon tumors.

(A) Representative immunofluorescence images of Tcon and Dcon tumor sections stained with anti-αSMA antibody. (B) Bar plot showing the average αSMA^{+}area per ROI in IF images of Tcon and Dcon tumors (n=8). The αSMA^{+}area were quantified via Image J. Bar plots showing qPCR results of (C) Acta2 and (D) Tgfb1 gene expression from RNA sample extracted from Tcon and Dcon tumors. Data from 3 biological repeats for Tcon tumor and Dcon tumors were analyzed. (E) Bar plot showing RNA-seq data of Wnt7a expression from RNA sample extracted from Tcon and Dcon cell (n=3). All data are presented as mean ± SEM. Unpaired t-test, $^{*}P < 0.05$, $^{**}P < 0.01$, $^{****}P < 0.0001$.

.

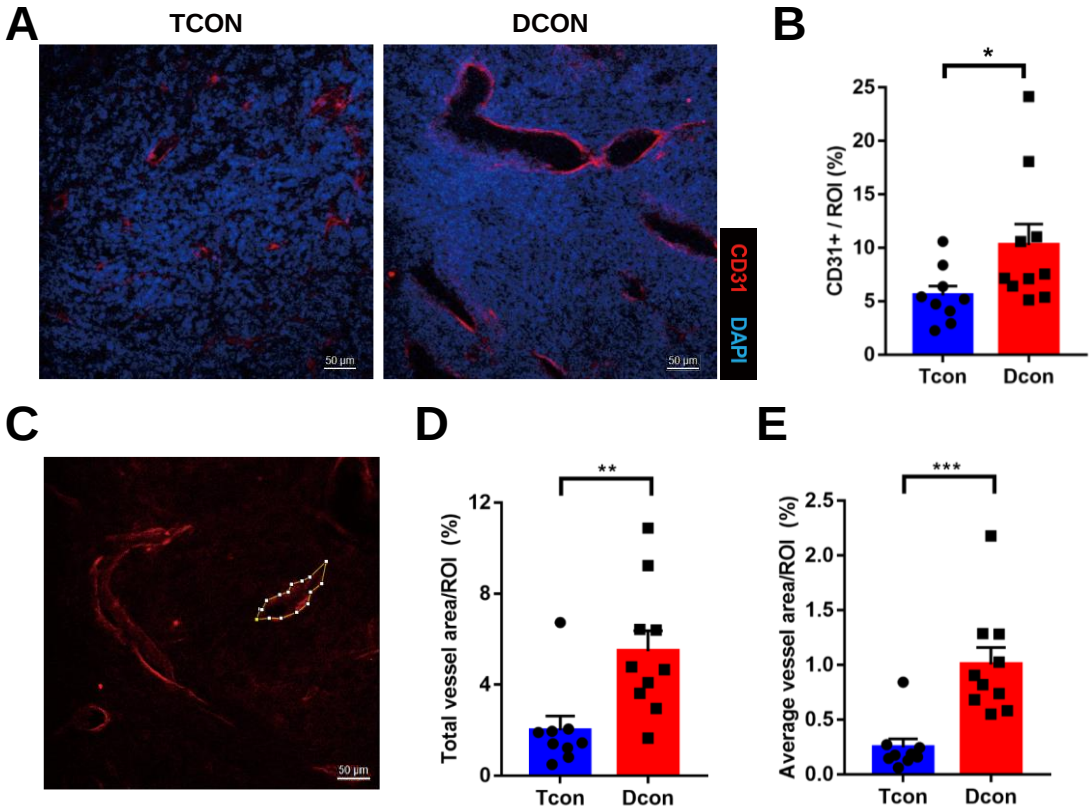

Figure 7. Tcon tumors display low vascularity with compressed blood vessels.

(A) Representative immunofluorescence images of Tcon and Dcon tumor sections stained with anti-CD31 antibody. (B) Bar plot showing $CD31^{+}$area per ROI in Tcon and Dcon tumors. (C) Representative method of measuring the area of each CD31-surrounding cavity that reflects the blood vessel. The area of the blood vessels is measured via Image J. Bar plots showing (D) total vessel area per ROI, (E) average vessel area per ROI in in Tcon and Dcon tumors. Data of 5 biological repeats from Tcon and Dcon tumors were analyzed. All data are presented as mean ± SEM. Unpaired t-test, $^{*}P < 0.05$, $^{**}P < 0.01$, $^{***}P < 0.001$.

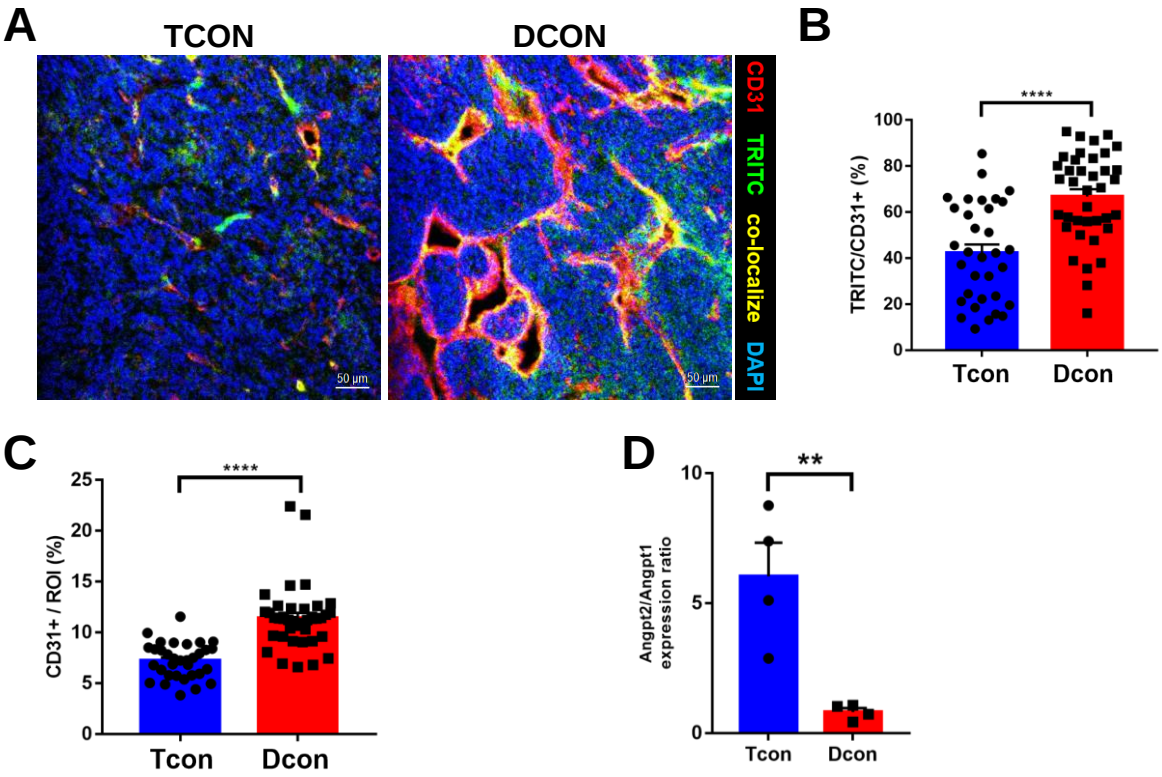

Figure 8. Tcon tumors show low vessel functionality.

(A) Representative immunofluorescence images of perfusion assay on Tcon and Dcon tumor sections after injection of 2000 kDa TRITC-dextran stained with anti-CD31 antibody. Red area shows $CD31^{+}$region, green area shows TRITC-localizing region, yellow area shows co-localizing region of CD31 and TRITC. Bar plots showing (B) TRITC-positive per $CD31^{+}$ area and (C) $CD31^{+}$area per ROI. Data of 6 biological repeats from Tcon and Dcon tumors were analyzed. (D) Bar plot showing ratio of Angpt2 expression to Angpt1 expression from RNA-seq data of Tcon and Dcon tumors (Tcon : n=4, Dcon : n=4). All data are presented as mean ± SEM. Unpaired t-test, $^{**}P < 0.01$, $^{***}P < 0.001$, $^{****}P < 0.0001$.

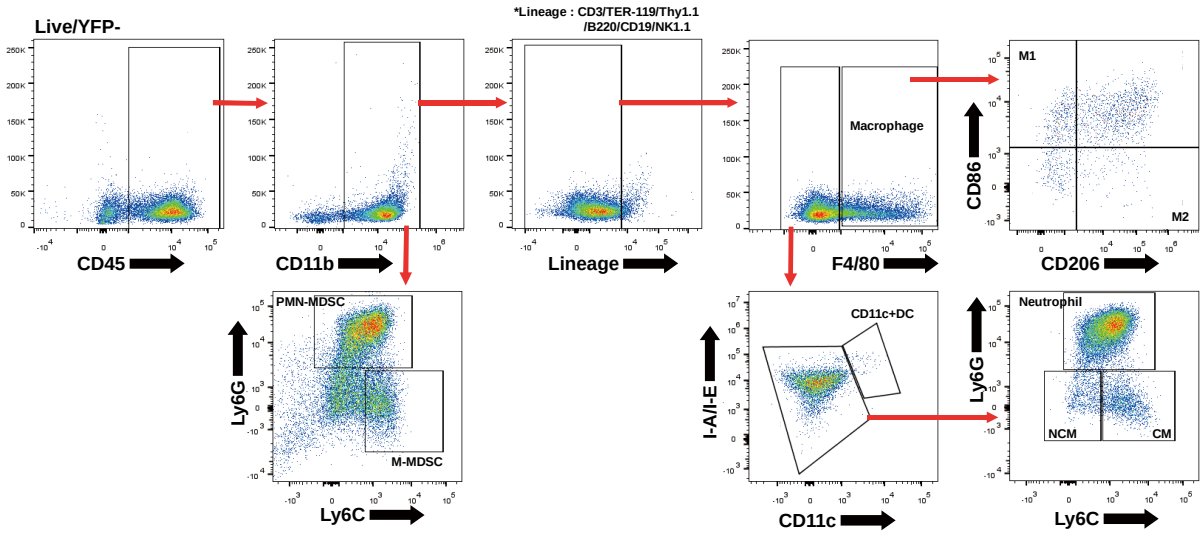

Figure 9. Gating strategy for flow cytometry analysis on myeloid subsets in Tcon and Dcon tumors.

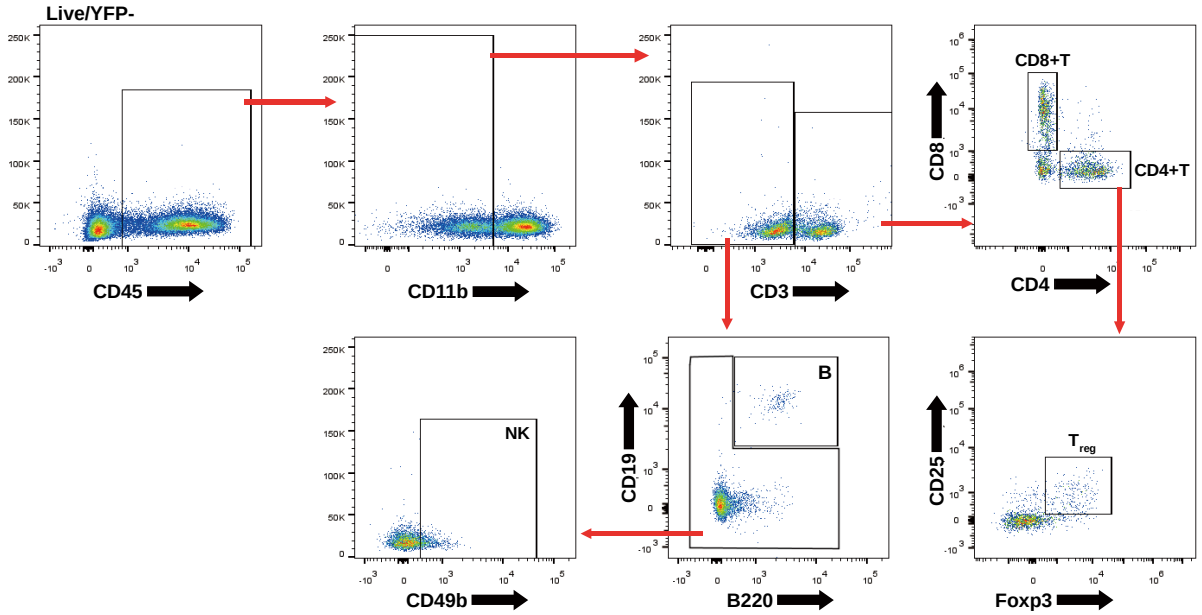

Figure 10. Gating strategy for flow cytometry analysis on lymphoid subsets in Tcon and Dcon tumors.

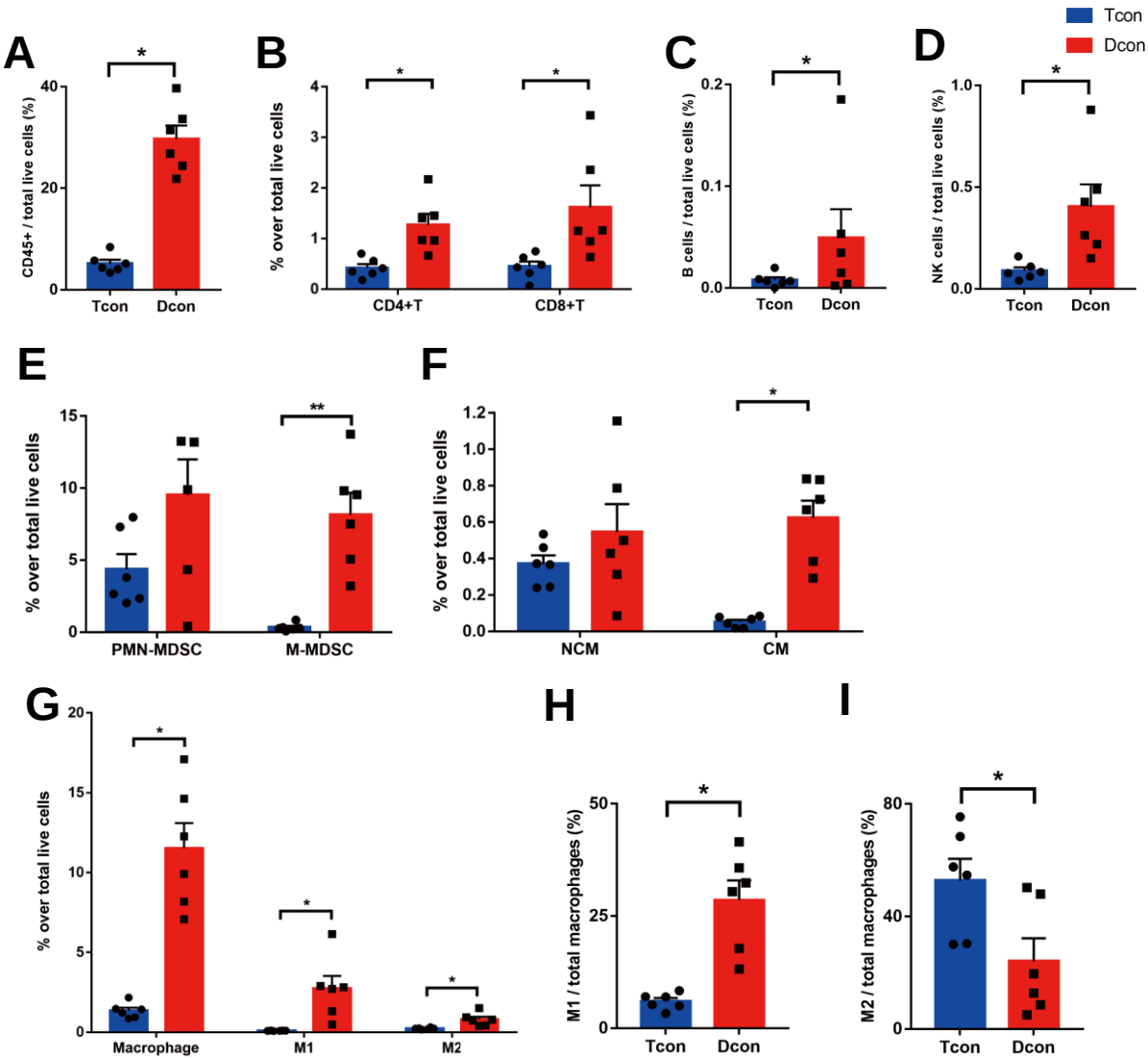

Figure 11. Dcon tumors displayed high immune cell infiltration and anti-tumoral effector cell population.

Bar plots showing (A) Total immune cells ($CD45^+$), (B) $CD4^+T$ cells and $CD8^+T$ cells, (C) B cells, (D) NK cells, (E) PMN-MDSCs and M-MDSCs, (F) Non-classical monocytes and Classical monocytes, (G) Macrophages with subtypes of M1-like ($CD86^+CD206^-$) and M2-like ($CD206^+CD86^-$). Bar plots showing M1 (Tcon : n=7, Dcon : n=6). All data are presented as mean ± SEM. Unpaired t-test, $^*P < 0.05$, $^{**}P < 0.01$

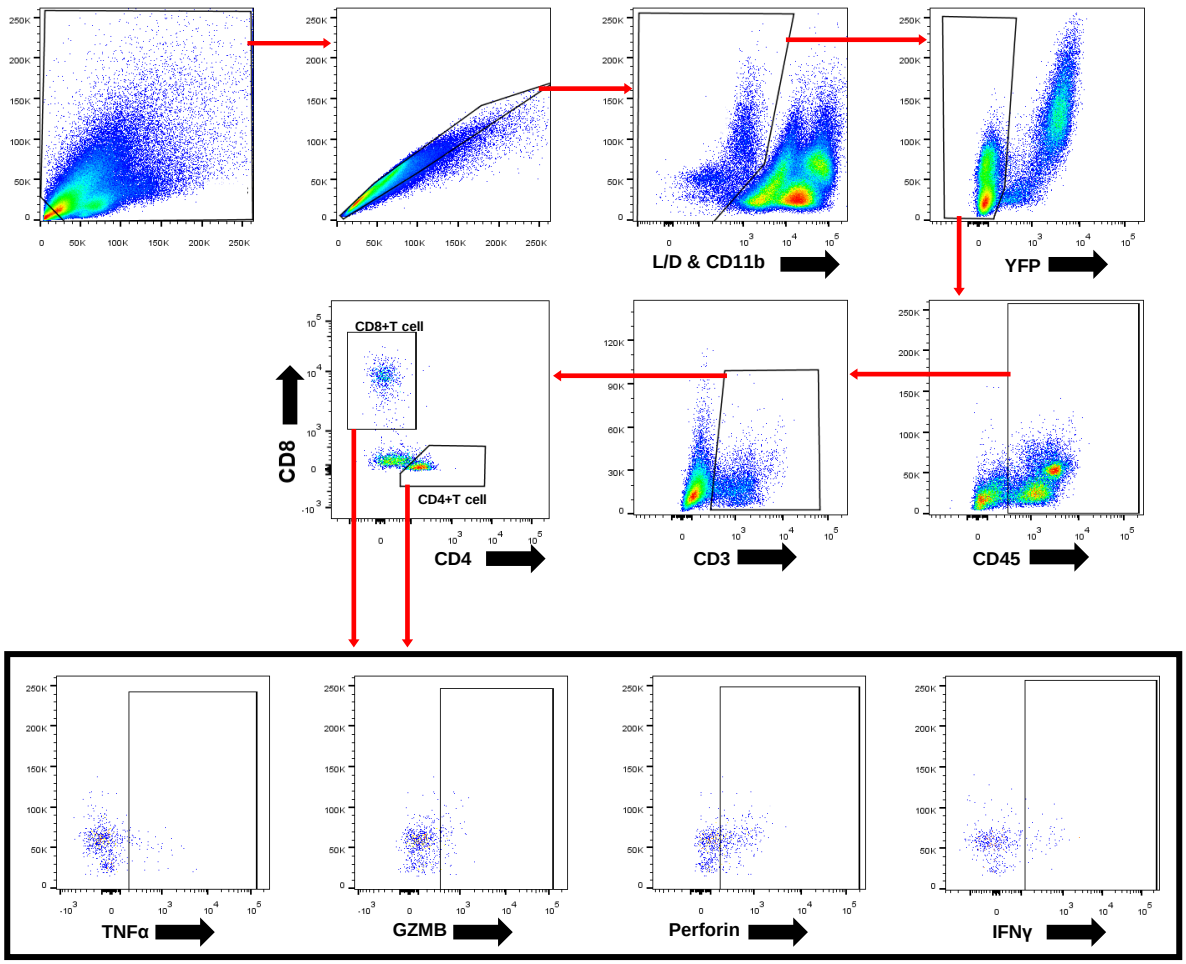

Figure 12. Gating strategy for flow cytometry analysis on cytokine producing T cells in Tcon and Dcon tumors.

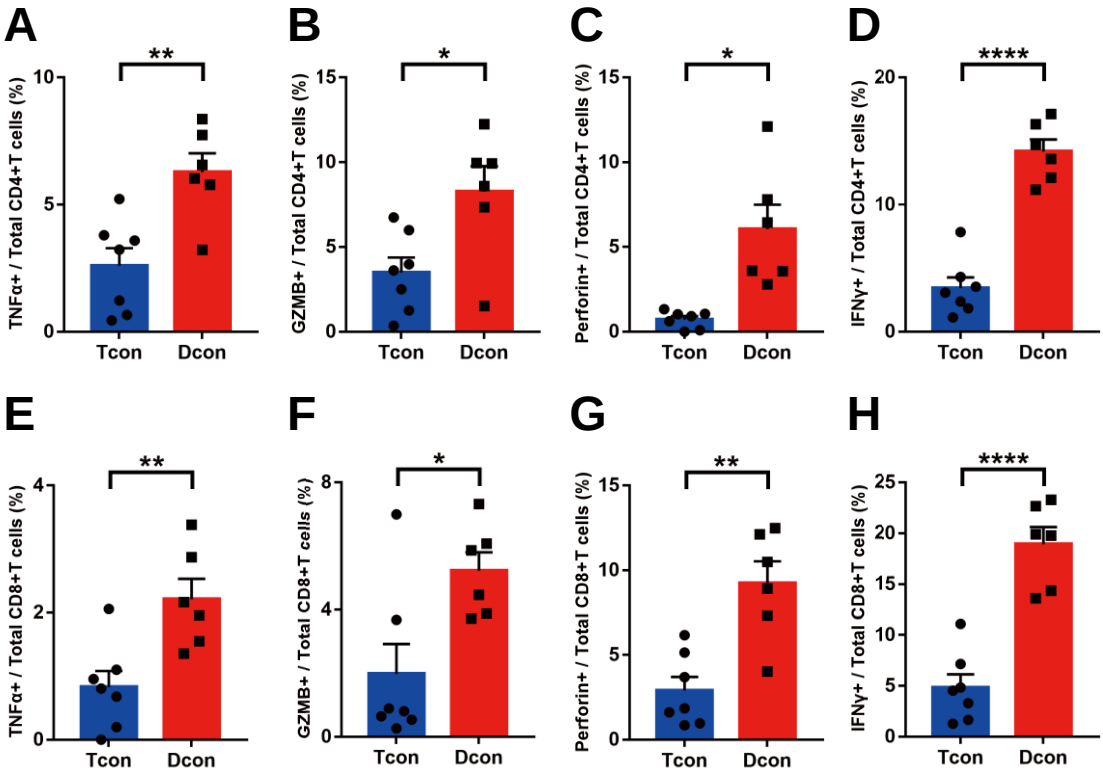

Figure 13. Dcon tumor displayed high effector T cell ratio.

Bar plots showing $CD4^{+}T$ cells producing (A) TNF α, (B) Granzyme B, (C) Perforin and (D) Interferon$-\gamma$ per total $CD4^{+}T$ cells. Bar plots showing $CD8^{+}T$ cells producing (E) TNF α, (F) Granzyme B, (G) Perforin and (H) Interferon$-\gamma$ per total $CD8^{+}T$ cells (Tcon : n=7, Dcon : n=6). All data are presented as mean ± SEM. Unpaired t-test, $^{*}P < 0.05$, $^{**}P < 0.01$, $^{****}P < 0.0001$.

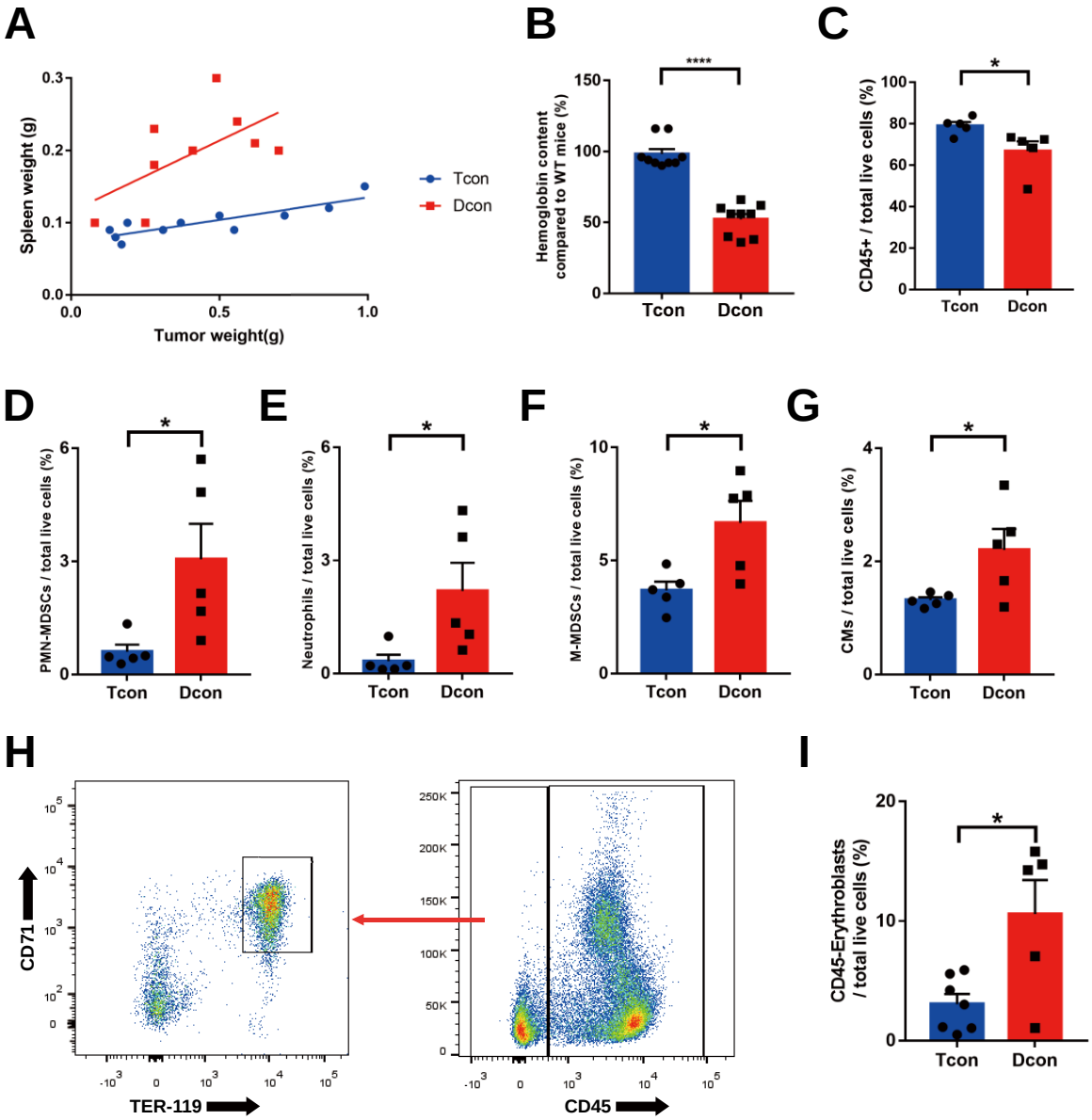

Figure 14. Dcon tumor bearing mice displayed severe splenomegaly, enriched with myeloid cells and erythroblasts.

(A) Dot plot showing Tcon and Dcon tumor weight in X axis, corresponding to the host' s spleen weight in Y axis with linear regression models for each tumor type. (B) Bar plot showing the hemoglobin content of blood from Tcon and Dcon tumor bearing mice compared to that from

WT mice measured via Drabkin’s reagent. Data from 3 biological repeats were analyzed. Bar plots showing cell populations of (C) total immune cells, (D) PMN-MDSCs, (E) Neutrophils, (F) M-MDSCs, (G) Classical monocytes per total live cells in spleens of Tcon and Dcon tumor bearing mice (H) Gating strategy for erythroid subsets in spleens of Tcon and Dcon tumor bearing mice. (I) Bar plot showing cell populations of $CD45^{-}$ Erythroblasts in spleens of Tcon and Dcon tumor bearing mice. (Tcon : n=7, Dcon : n=6). All data are presented as mean ± SEM. Unpaired t-test, $^{*}P < 0.05$, $^{****}P < 0.0001$.

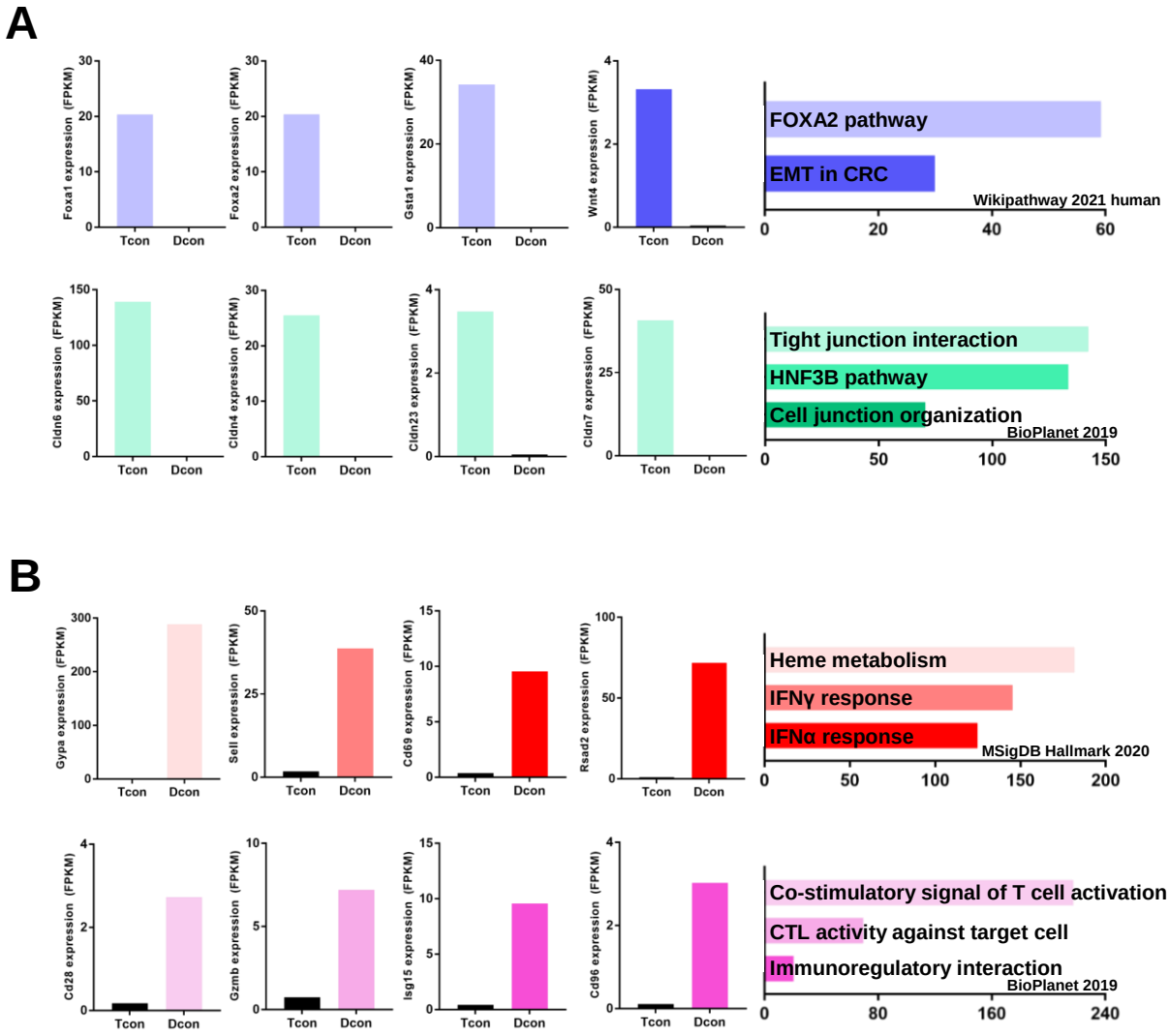

Figure 15. RNA-sequencing of Tcon and Dcon tumors reveal differentially enriched biological pathways.

Bar plots of representative DEGs (Left) corresponding to the identical color of enriched pathways (Right) from gene set enrichment analysis (GSEA) of (A) Tcon and (B) Dcon tumors.

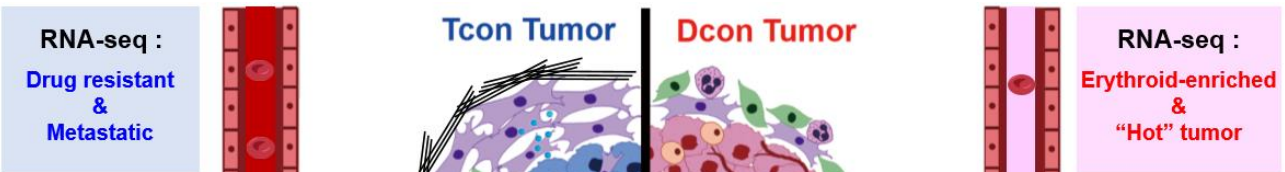

Figure 16. Distinct phenotypes of tumor micro-environment and macro-environment in Tcon and Dcon cells.

DISCUSSION

The study successfully identified phenotypic differences between Tcon and Dcon gastric tumor models. Tcon tumors exhibited desmoplasia and vascular compression, while Dcon tumors showed extensive angiogenesis and immune cell infiltration. Severe fibrosis occurred in Tcon tumors due to αSMA single-positive cancer-associated fibroblasts (CAFs), while vessel compression suppressed functional blood vessel formation in Dcon tumors. Dcon tumors also exhibited tumor-associated anemia and splenomegaly, with enrichment of myeloid subsets and erythroblasts in the enlarged spleen. Furthermore, Dcon tumors had high immune cell infiltration, including effector T cells expressing anti-tumoral cytokines. The study suggests that specific CAF subsets and immune cells may play a role in modulating the tumor microenvironment in Tcon and Dcon tumors.

Despite Tcon tumors lacking E-Cadherin expression, a tumor suppressor protein, and Dcon tumors having high immune cell infiltration and effector T cell ratio, it was intriguing that Dcon tumors outgrew Tcon tumors after Day 25-28. The stress from desmoplastic stroma in Tcon tumors could explain this unexpected phenomenon, as fibrotic stroma can exert compression on tumors, limiting their growth (79-82). However, tumor cells in response to this mechanical stress can undergo epithelial-mesenchymal

transition (EMT) and invade adjacent organs or metastasize, which is consistent with Tcon TG mice that displayed extensive metastasis in Till et al (9,83-84). In contrast, Dcon tumors with better vascularization and higher blood perfusion facilitate immune cell infiltration, oxygen supply, and nutrient delivery, supporting their rapid growth. RNA-seq data suggests upregulation of genes related to carbohydrate and protein metabolism in Dcon tumors, further contributing to their growth (85-86). Sine my immune profiling data were originated from tumors at Day 28, Future studies should investigate immune cell infiltration, effector T cell ratio, and tumor vascularization at different time points, particularly in late-stage tumors, to understand fluctuations in anti-tumor immunity in Dcon tumors.

Tcon tumors are expected to display low efficacy of chemotherapy or immunotherapy treatment. Thus, treatment of collagenase (87), or immunotherapy that targets CAF subsets that induce desmoplasia in Tcon tumors including αSMA single-positive CAFs or inhibitors of CAF activation such as Losartan, Pentoxifylline, Metformin are expected to relieve the severe desmoplasia in Tcon tumors, that would eventually enhance the drug delivery (88-90), and ultimately induce the tumor regression by combinatorial therapy with traditional chemotherapy.

Meanwhile, Dcon tumors are expected to display favorable drug delivery due to the well-vascularized TME, with higher extent of immune cell infiltration including effector T cells supposedly activated with supports of M1-lilke macrophages.

However, in another point view, effector T cells producing IFN-γ and TNFα could also polarize and activate M1-like macrophage, since M1 type macrophages are well-known to be polarized by secreted cytokines mentioned above (91-92). Thus, it could be quite confusing whether effector T cells activated M1-like macrophage or vice versa, nor it is clear if the long-hold immunological notion that activation of innate immunity takes place in advance to that of adaptive immunity applies to the Dcon tumors. However, it is of importance that reciprocal interaction between M1-like macrophages and effector T cells can occur to potentiate anti-tumor immunity in Dcon tumors.

Nevertheless, validation of M1-like and M2-like macrophages genuinely reflect the well-known phenotypes of M1 and M2 type macrophages is required. Substantial researches have elucidated that single cell RNA-sequencing analysis on Tumor-associated macrophages (TAMs) reveals that M1/M2 type markers or common M1/M2 associated genes cannot distinguish M1 and M2 type macrophages among the heterogeneous clusters of TAMs (93-95). For example, M2 type macrophages are known to be pro-tumoral, with their immunosuppressive abilities, however, $C1QC^{+}$ macrophages, which also expressed CD206 in colorectal tumors were, in fact, "anti-tumoral" (93). It has been reported that some subtypes of TAMs do not express M1/M2-related marker genes at all, while some of the others express both of M1 and M2-related marker genes (94-95). Therefore, for accurate estimation of anti-tumor immunity induced by macrophages in tumors, definition of

pro-tumoral or anti-tumoral subtypes based on functional markers should be established or functional analysis including depletion study and co-culture experiment with cytotoxic lymphocytes are required.

Furthermore, spleens of Dcon tumor bearing mice were enriched with myeloid cells and erythroblasts. Tumor infiltrating myeloid cells are known to act as major regulator that promotes tumor progression through immune suppression and tumor angiogenesis. On the other hand, tumor-associated splenic erythroblasts are also reported to induce tumor progression in various means, including secretion of pro-tumoral factors, and suppressing the anti-tumor immunity by entering the tumor. Therefore, inhibition of myelopoiesis and erythropoiesis in the spleen or splenectomy is expected to block the migration of pro-tumoral cells into the tumor to suppress the tumor progression (58,96)

Thus, for clinical application of these therapeutic strategies, it is important to associate Tcon and Dcon tumor to clinically relevant human cancer types based on genotypic and phenotypic characteristics.

Loss of E-Cadherin has been observed in various cancer types, including medullary thyroid cancer, cutaneous melanoma, metastatic lobular mammary carcinoma, and gastric cancer, leading to the development of desmoplasia (97-100). Mouse models and patient-derived xenograft (PDX) models have also demonstrated similar phenotypes in lung adenocarcinoma and scirrhous gastric cancer, respectively (101-103). However, DCKO mice (Atp4b-Cre;

Trp53$^{fl/fl}$; CDH1$^{fl/fl}$), gastric tumor model introduced in Shimada et al., sharing genetic background with Tcon mice except for oncogenic activation of Kras gene, also displayed linitis plastica in stomach with tumor cells surrounded by αSMA^{+} myofibroblasts, leaving oncogenic Kras as a dispensable factor for desmoplastic reaction in Tcon tumors (100). Meanwhile, CKO mice (Atp4b-Cre; CDH1$^{fl/fl}$) did not show tumorigenesis, implicating that loss of E-Cadherin alone isn't sufficient for gastric tumorigenesis, however, combination with p53 induce desmoplastic tumor (100). However, oncogenic Kras activation facilitates rapid tumor progression, since 100% of Tcon mice in Till et al. died in 91 days after cancer initiation, however, 50% DCKO mice in Shimada et al. survived after 12 months of tumor initiation (100). Thus, SGC, a desmoplastic subtype of diffuse-type gastric cancer, with oncogenic Kras activation, despite of its rare occurrence, could be represented by Tcon tumors (104).

On the other hand, intestinal type gastric cancer is known to overlap with Chromosomal Instability (CIN) type, which share abundant mutation of p53 and alteration of Ras-RTK pathway including oncogenic Kras, while rarely possess E-Cadherin mutation (105). Interestingly, soluble form of extracellular domain of E-Cadherin, cleaved by ADAM and MMP family, has been reported to bind to Epidermal growth factor receptor (EGFR) and promote downstream pathways including RAS and PI3K (106-107). Furthermore, several reports of immune cell infiltration into gastric tumor revealed that intestinal type gastric cancer is more likely to

show larger TIL population, compared to diffuse-type gastric cancer, which might be associated to better prognosis (108-109). Therefore, Dcon tumors could reflect intestinal type gastric cancer with higher immune cell infiltration.

The present study, however, have several limitations. To begin with, relationship between expression or loss of E-cadherin and phenotypic differences of Tcon or Dcon tumors are insufficient. The difference between Tcon and Dcon tumors were derived from differential mutation on single copy of Cdh1 gene, thus, it is important to figure out the function of E-Cadherin.

One possible suggestion is that activation of Wnt/β-catenin pathway due to loss of E-Cadherin has been reported to induce Shh expression in studies of development (110-111). In other studies, Shh signaling was confirmed to promote recruitment and activation of myofibroblastic CAF and induce desmoplasia in PDAC (112-114). Since RNA-seq data also state that Shh is highly upregulated in Tcon tumors, the suggestion could be worth to be verified.

Meanwhile, soluble E-Cadherin was confirmed to promote tumor angiogenesis in ovarian cancer via binding to VE-Cadherin on endothelial cells as ligand molecule, and activate NF-kB pathway (14). Since Dcon tumors retain a single copy of wild type E-Cadherin allele, and were shown to be well-vascularized, angiogenic function of cleaved E-Cadherin is to be validated.

Moreover, subcutaneous tumor models utilized in the present study cannot fully reflect the TME of GC, since Tcon and Dcon cells are derived from the stomach of Tcon and Dcon TG mice. Additionally,

tumors in stomach of Tcon TG mice displayed higher incidence of metastasis to lung and liver (9), however, subcutaneous tumors in the present study rarely showed signs of metastasis. Hence, establishing the orthotopic gastric tumor model for Tcon and Dcon tumors are essential for better reflection of the TME of GC.

REFERENCES

1. https://gco.iarc.fr/today
2. Lauren, P. The two histological main types of gastric carcinoma: Diffuse and so-called intestinal-type carcinoma. An attempt at a histo-clinical classification. Acta Pathol. Microbiol. Scand. 1965, 64, 31-49.
3. Zheng HC, Li XH, Hara T et al. Mixed type gastric carcinoma exhibit more aggressive features and indicate the histogenesis of carcinomas. Virchows Arch. 2008, 452(5):525-534.
4. Smyth, E. C. et al. Gastric cancer. Lancet (Lond., Engl.). 2020, 396, 635-648
5. Allemani C, et al. Global surveillance of trends in cancer survival 2000-14 (CONCORD-3): analysis of individual records for 37 513 025 patients diagnosed with one of 18 cancers from 322 population-based registries in 71 countries. Lancet. 2018, 391(10125):1023-75.
6. Roma-Rodrigues, C., Mendes, R., Baptista, P. V. & Fernandes, A. R. Targeting tumor microenvironment for cancer therapy. Int. J. Mol. Sci. 2019, 20, 840.
7. L. Bejarano, M. J. C. Jordāo, and J. A. Joyce, Therapeutic Targeting of the Tumor Microenvironment. Cancer Discov. 2021, 11, 933.
8. Petitprez F, Meylan M, de Reyniès A, Sautès-Fridman C, Fridman WH. The Tumor Microenvironment in the response to Immune Checkpoint Blockade Therapies. Front Immunol. 2020, 11:784.
9. J.E. Till, C. Yoon, B.J. Kim, K. Roby, P. Addai, E. Jonokuchi, L.H. Tang, S.S. Yoon, S. Ryeom, Oncogenic KRAS and p53 loss drive gastric tumorigenesis in mice that can be attenuated by E-

cadherin expression, Cancer Res. 2017, 5349-5359.

10. J. Di Gregorio, I. Robuffo, S. Spalletta, G. Giambuzzi, V. De Iuliis, E. Toniato, S. Martinotti, P. Conti, V. Flati, The epithelial-to-mesenchymal transition as a possible therapeutic target in fibrotic disorders, Front. Cell. Dev. Biol. 2020, 8, 607483.
11. Ansari, S.; Gantuya, B.; Tuan, V.P.; Yamaoka, Y. Diffuse Gastric Cancer: A Summary of Analogous Contributing Factors for Its Molecular Pathogenicity. Int. J. Mol. Sci. 2018, 19, 2424.
12. Mendonsa, A.M.; Na, T.Y.; Gumbiner, B.M. E-cadherin in contact inhibition and cancer. Oncogene. 2018, 37, 4769-4780.
13. Wong, S.H.M.; Fang, C.M.; Chuah, L.H.; Leong, C.O.; Ngai, S.C. E-cadherin: Its dysregulation in carcinogenesis and clinical implications. Crit. Rev. Oncol. Hematol. 2018, 121, 11-22.
14. Tang, M.K.; Yue, P.Y.; Ip, P.P.; Huang, R.-L.; Lai, H.-C.; Cheung, A.N.; Tse, K.Y.; Ngan, H.Y.; Wong, A.S. Soluble E-cadherin promotes tumor angiogenesis and localizes to exosome surface. Nat. Commun. 2018, 9, 2270.
15. Zeltz, C. et al. Cancer-associated fibroblasts in desmoplastic tumors: emerging role of integrins. Semin Cancer Biol. 2019, 08, 004
16. Li Z, Liu Z, Shao Z, Li C, Li Y, Liu Q, et al. Identifying multiple collagen gene family members as potential gastric cancer biomarkers using integrated bioinformatics analysis. PeerJ. 2020, 8:e9123.
17. Inoue T, Chung YS, Yashiro M, Nishimura S, Hasuma T, Otani S, et al. Transforming growth factor-beta and hepatocyte growth factor produced by gastric fibroblasts stimulate the invasiveness of scirrhous gastric cancer cells. Jpn J Cancer Res. 1997, 88(2):152-

9.

18. Yoshida K, Yokozaki H, Niimoto M, Ito H, Ito M, Tahara E. Expression of TGF-beta and procollagen type I and type III in human gastric carcinomas. Int J Cancer. 1989, 44(3):394-8.

19. Barsky, S. H., Green, W. R., Grotendorst, G. R. & Liotta, L. A. Desmoplastic breast carcinoma as a source of human myofibroblasts. Am. J. Pathol. 1984, 115, 329-333.

20. Elenbaas, B. & Weinberg, R. A. Heterotypic signaling between epithelial tumor cells and fibroblasts in carcinoma formation. Exp. Cell Res. 2001, 264, 169-184.

21. Daniel Öhlund. Distinct populations of inflammatory fibroblasts and myofibroblasts in pancreatic cancer. JEM. 2017, 214(3): 579-596.

22. Kim, D.K., Jeong, J., Lee, D.S. et al. PD-L1-directed PlGF/VEGF blockade synergizes with chemotherapy by targeting $CD141^{+}$ cancer-associated fibroblasts in pancreatic cancer. Nat Commun. 2022, 13, 6292.

22. Elyada E, Bolisetty M, Laise P, Flynn WF, Courtois ET, Burkhart RA, Teinor JA, Belleau P, Biffi G, Lucito MS, Sivajothi S, Armstrong TD, Engle DD, Yu KH, Hao Y, Wolfgang CL, Park Y, Preall J, Jaffee EM, Califano A, Robson P, Tuveson DA. Cross-species single-cell analysis of pancreatic ductal adenocarcinoma reveals antigen-presenting cancer-associated fibroblasts. Cancer Discov. 2019, 9: 1102-1123

23. Bartoschek M, Oskolkov N, Bocci M, Lövrot J, Larsson C, Sommarin M, Madsen CD, Lindgren D, Pekar G, Karlsson G, Ringnér M, Bergh J, Björklund Å, Pietras K. Spatially and functionally distinct subclasses of breast cancer-associated fibroblasts revealed by single cell RNA sequencing. Nat Commun.

2018, 9: 5150.

24. McAnulty, R. J. Fibroblasts and myofibroblasts: their source, function and role in disease. Int. J. Biochem. Cell Biol. 2007, 39, 666-671.
25. Petersen OW, Nielsen HL, Gudjonsson T, Villadsen R, Rank F, Niebuhr E, et al. Epithelial to mesenchymal transition in human breast cancer can provide a nonmalignant stroma. Am J Pathol 2003, 162(2):391-402.
26. Oft M, Akhurst RJ, Balmain A. Metastasis is driven by sequential elevation of H-ras and Smad2 levels. Nat Cell Biol 2002, 4(7):487-94.
27. Spano, C., Grisendi, G., Golinelli, G., Rossignoli, F., Prapa, M., Bestagno, M., et al. Soluble TRAIL armed human MSC as gene therapy for pancreatic cancer. Sci. Rep. 2019, 9:1788.
28. Liu, T., Han, C., Wang, S., Fang, P., Ma, Z., Xu, L., et al. Cancer-associated fibroblasts: an emerging target of anti-cancer immunotherapy. J. Hematol. Oncol. 2019, 12:86.
29. Jotzu C, Alt E, Welte G, Li J, Hennessy BT, Devarajan E, et al. Adipose tissue derived stem cells differentiate into carcinoma-associated fibroblast-like cells under the influence of tumor-derived factors. Anal Cell Pathol (Amst) 2010, 33(2):61-79.
30. Bochet, L., Lehuédé, C., Dauvillier, S., Wang, Y. Y., Dirat, B., Laurent, V., et al. Adipocyte-derived fibroblasts promote tumor progression and contribute to the desmoplastic reaction in breast cancer. Cancer Res. 2013, 73, 5657-5668.
31. Koopmans, T., and Rinkevich, Y. Mesothelial to mesenchyme transition as a major developmental and pathological player in trunk organs and their cavities. Commun. Biol. 2018, 1:170.

32. H. Huang, Z. Wang, Y. Zhang, R.N. Pradhan, D. Ganguly, R. Chandra, G. Murimwa, S. Wright, X. Gu, R. Maddipati, S. Muller, S.J. Turley, R.A. Brekken, Mesothelial cell-derived antigen-presenting cancer-associated fibroblasts induce expansion of regulatory T cells in pancreatic cancer, Cancer Cell. 2022, 40, 656-673.e7.
33. Hosaka, K., Yang, Y., Seki, T., Fischer, C., Dubey, O., Fredlund, E., et al. Pericyte-fibroblast transition promotes tumor growth and metastasis. Proc. Natl. Acad. Sci. U.S.A. 2016, 113, E5618-E5627.
34. Ino, K., Masuya, M., Tawara, I., Miyata, E., Oda, K., Nakamori, Y., et al. Monocytes infiltrate the pancreas via the MCP-1/CCR2 pathway and differentiate into stellate cells. PLoS One. 2014, 9:e84889.
35. N.I. Nissen, M. Karsdal, N. Willumsen, Collagens and Cancer associated fibroblasts in the reactive stroma and its relation to Cancer biology, Journal of Experimental & Clinical Cancer Research. 2019, 38, 1-12.
36. Dvorak, H. F. Tumors: wounds that do not heal. Similarities between tumor stroma generation and wound healing. N. Engl. J. Med. 1986, 315, 1650-1659.
37. Bu, L.; Baba, H.; Yasuda, T.; Uchihara, T.; Ishimoto, T. Functional diversity of cancer-associated fibroblasts in modulating drug resistance. Cancer Sci. 2020, 111, 3468-3477.
38. Ham I-H, Lee D, Hur H. Cancer-associated fbroblast-induced resistance to chemotherapy and radiotherapy in gastrointestinal cancers. Cancers (basel). 2021, 13:1172.
39. Miki Y, Yashiro M, Okuno T, Kitayama K, Masuda G, Hirakawa K, et al. CD9-positive exosomes from cancerassociated fibroblasts stimulate the migration ability of scirrhous-type gastric cancer

cells. Br J Cancer. 2018, 118:867-77.

40. Xu G, Zhang B, Ye J, Cao S, Shi J, Zhao Y, et al. Exosomal miRNA-139 in cancer-associated fibroblasts inhibits gastric cancer progression by repressing mmp11 expression. Int J Biol Sci. 2019, 15:2320-9.
41. Guo J, Miao Y, Xiao B, Huan R, Jiang Z, Meng D, Wang Y. Differential expression of microRNA species in human gastric cancer versus non-tumorous tissues. J Gastroenterol Hepatol. 2009, 24: 652-657
42. Seok JK, Lee SH, Kim MJ, Lee YM. MicroRNA-382 induced by HIF-1α is an angiogenic miR targeting the tumor suppressor phosphatase and tensin homolog. Nucleic Acids Res. 2014, 42: 8062-8072
43. Miyai, Y.; Esaki, N.; Takahashi, M.; Enomoto, A. Cancer-associated fibroblasts that restrain cancer progression: Hypotheses and perspectives. Cancer Sci. 2020, 111, 1047-1057.
44. Hanahan D, Folkman J. Patterns and emerging mechanisms of the angiogenic switch during tumorigenesis. Cell. 1996, 86: 353-64.
45. Folkman J. Tumor angiogenesis: therapeutic implications. N Engl J Med. 1971, 285: 1182-6.
46. Ghiabi P, Jiang J, Pasquier J et al. Endothelial cells provide a notch-dependent pro-tumoral niche for enhancing breast cancer survival, stemness and pro-metastatic properties. PLoS One. 2014, 9: e112424.
47. Chang YS, di Tomaso E, McDonald DM, Jones R, Jain RK, Munn LL. Mosaic blood vessels in tumors: frequency of cancer cells in contact with flowing blood. Proc Natl Acad Sci USA. 2000, 97: 14608-13.

48. Wong PP, Demircioglu F, Ghazaly E, Alrawashdeh W, Stratford MR, Scudamore CL, et al.. Dual-action combination therapy enhances angiogenesis while reducing tumor growth and spread. Cancer Cell. 2015, 27:123-37.
49. S. Azzi, J.K. Hebda, J. Gavard, Vascular permeability and drug delivery in cancers, Front. Oncol. 2013, 3, 211.
50. Jain RK. Antiangiogenesis strategies revisited: from starving tumors to alleviating hypoxia. Cancer Cell. 2014, 26(5):605-22.
51. Wei Q, Frenette PS. Niches for hematopoietic stem cells and their progeny. Immunity. 2018, 48:632-48.
52. Gabrilovich DI, Ostrand-Rosenberg S, Bronte V. Coordinated regulation of myeloid cells by tumours. Nat Rev Immunol. 2012, 12:253-68.
53. Kumar V, Patel S, Tcyganov E, Gabrilovich DI. The nature of myeloid-derived suppressor cells in the tumor microenvironment. Trends Immunol. 2016, 37:208-20.
54. Abdel-Wahab OI, Levine RL. Primary myelofibrosis: update on definition, pathogenesis, and treatment. Annu Rev Med. 2009, 60:233-45.
55. Cheshier SH, Prohaska SS, Weissman IL. The effect of bleeding on hematopoietic stem cell cycling and self-renewal. Stem Cells Dev. 2007, 16:707-17.
56. Bayne LJ, Beatty GL, Jhala N, Clark CE, Rhim AD, Stanger BZ, et al. Tumor-derived granulocyte-macrophage colony-stimulating factor regulates myeloid inflammation and T cell immunity in pancreatic cancer. Cancer Cell. 2012, 21:822-35.
57. Han Y, Liu Q, Hou J, Gu Y, Zhang Y, Chen Z, et al. Tumor-induced generation of splenic erythroblast-like ter-cells promotes tumor

progression. Cell. 2018, 19;173(3):634-648.e12.

58. Hao Z, Guang-zhi W, Yu-ying W, Wen C, Jing-Zhi G et al. The role of erythrocytes and erythroid progenitor cells in tumors. Open Life Sciences. 2022, 1641-1656.

59. Wu C, Hua Q, Zheng L. Generation of myeloid cells in cancer: The spleen matters. Front Immunol. 2020, 11:1126.

60. Cho YA, Yoon HJ, Lee JI, Hong SP, Hong SD. Relationship between the expressions of PD-L1 and tumor-infiltrating lymphocytes in oral squamous cell carcinoma. Oral Oncol. 2011, 47:1148-53.

61. Planes-Laine G, Rochigneux P, Bertucci F et al. PD-1/PD-L1 targeting in breast cancer: the frst clinical evidences are emerging. A Lit Rev Cancers. 2019, 11(7):1033.

62. Eikenes, L., Bruland, O. S., Brekken, C., and Davies Cde, L. Collagenase increases the transcapillary pressure gradient and improves the uptake and distribution of monoclonal antibodies in human osteosarcoma xenografts. Cancer Res. 2004, 64, 4768-4773.

63. Huang, H., Bhat, A., Woodnutt, G. et al. Targeting the ANGPT-TIE2 pathway in malignancy. Nat Rev Cancer. 2010, 10, 575–585.

64. Xie Z, Bailey A, Kuleshov MV, Clarke DJB., Evangelista JE, Jenkins SL, Lachmann A, Wojciechowicz ML, Kropiwnicki E, Jagodnik KM, Jeon M, & Ma'ayan A. Gene set knowledge discovery with Enrichr. Current Protocols. 2021, 1, e90.

65. Wang B, Liu G, Ding L, Zhao J, Lu Y et al. FOXA2 promotes the proliferation, migration and invasion, and epithelial mesenchymal transition in colon cancer. Exp Ther Med. 2018, 16: 133-140.

66. Gao, H., Yan, Z., Sun, H. et al. FoXA2 promotes esophageal squamous cell carcinoma progression by ZEB2 activation. World J

Surg Onc. 2021, 19, 286.

67. Liu H, Yang Z, Zang L, Wang G, Zhou S, Jin G, Yang Z, Pan X. Downregulation of Glutathione S-transferase A1 suppressed tumor growth and induced cell apoptosis in A549 cell line. Oncol Lett. 2018, 16(1):467-474.

68. Liu X, Sui X, Zhang C, Wei K, Bao Y, Xiong J, Zhou Z, Chen Z, Wang C, Zhu H, Tang F. Glutathione S-transferase A1 suppresses tumor progression and indicates better prognosis of human primary hepatocellular carcinoma. J Cancer. 2020, 1;11(1):83-91.

69. Yu, S., Zhang, Y., Li, Q. et al. CLDN6 promotes tumor progression through the YAP1-snail1 axis in gastric cancer. Cell Death Dis. 2019, 10, 949.

70. Hicks, D.A., Galimanis, C.E., Webb, P.G. et al. Claudin-4 activity in ovarian tumor cell apoptosis resistance and migration. BMC Cancer. 2016, 16, 788.

71. C. Breed, D.A. Hicks, P.G. Webb, C.E. Galimanis, B.G. Bitler, K. Behbakht, H.K. Baumgartner, Ovarian tumor cell expression of claudin-4 reduces apoptotic response to paclitaxel, Mol. Cancer Res. 2019, 17. 741e750.

72. Chen J, Qiao YD, Li X, Xu JL, Ye QJ, Jiang N, Zhang H, Wu XY. Intratumoral CD45+CD71+ erythroid cells induce immune tolerance and predict tumor recurrence in hepatocellular carcinoma. Cancer Lett. 2021, 28;499:85-98.

73. Su M, Lin Y, Cui C, Tian X, Lai L. ERMAP is a B7 family-related molecule that negatively regulates T cell and macrophage responses. Cell Mol Immunol. 2021,18(8):1920-1933.

74. Wang Y, Xiang X, Chen H, Zhou L, Chen S, Zhang G, Liu X, Ren X, Liu J, Kuang M, Jiang J, She J, Zhang Z, Xue R, Jiang H, Wang J,

Peng S. Intratumoral erythroblastic islands restrain anti-tumor immunity in hepatoblastoma. Cell Rep Med. 2023, 16;4(5):101044.

75. Jorgovanovic, D., Song, M., Wang, L. et al. Roles of IFN-γ in tumor progression and regression: a review. 2020, Biomark Res 8, 49.

76. Lu C, Klement JD, Ibrahim ML, Xiao W, Redd PS, Nayak-Kapoor A, Zhou G, Liu K. Type I interferon suppresses tumor growth through activating the STAT3-granzyme B pathway in tumor-infiltrating cytotoxic T lymphocytes. J Immunother Cancer. 2019, 22;7(1):157.

77. Yi M., Niu M., Xu Li. et al. Regulation of PD-L1 expression in the tumor microenvironment. J Hematol Oncol. 2021, 14, 10.

78. Feng, S. Isayev, O. Werner, J. Bazhin, A.V. CD96 as a Potential Immune Regulator in Cancers. Int. J. Mol. Sci. 2023, 24, 1303.

79. Fang M., Yuan J., Peng C. et al. Collagen as a double-edged sword in tumor progression. Tumor Biol. 2014, 35, 2871–2882

80. P Maneshi., J Mason., M Dongre., D Öhlund. Targeting tumor-stromal interactions in pancreatic cancer: impact of collagens and mechanical traits . Front. Cell Dev. Biol. 2021, 9

81. Josette M., D Ivory S., Janna K M., Wr Valerie M. Feeling Stress: The Mechanics of Cancer Progression and Aggression. Front. Cell Dev. Biol. 2018, 6

82. Helmlinger G., Netti P., Lichtenbeld H. Solid stress inhibits the growth of multicellular tumor spheroids. Nat Biotechnol. 1997, 15, 778–783

83. Yu H., Janna K M., and Valerie M. W., Forcing form and

function: biomechanical regulation of tumor evolution. Trends in cell biology. 2011, 21.1 :47-56.

84. Torzilli, P. A., Bourne, J. W., Cigler, T., Vincent, C. T. A new paradigm for mechanobiological mechanisms in tumor metastasis. Seminars in cancer biology. 2012, 22, 5-6, 385-395.

85. Yang Z., Zhuan B., Yan Y., Jiang S., Wang T. Integrated analyses of copy number variations and gene differential expression in lung squamous-cell carcinoma. Biological research. 2015, 48, 1-8.

86. Xu Q., Chen J., Ni S., Tan C., Xu M., Dong L., ... Du X. Pan-cancer transcriptome analysis reveals a gene expression signature for the identification of tumor tissue origin. Modern Pathology. 2016, 29(6), 546-556.

87. Stylianopoulos T, Martin JD, Chauhan VP, Jain SR, Diop-Frimpong B, Bardeesy N, Smith BL, Ferrone CR, Hornicek FJ, Boucher Y, Munn LL, Jain RK. Causes, consequences, and remedies for growth-induced solid stress in murine and human tumors. Proc Natl Acad Sci USA. 2012, 109: 15101-15108.

88. Kim JH, Shin BC, Park WS, Lee J, Kuh HJ. Antifibrotic effects of pentoxifylline improve the efficacy of gemcitabine in human pancreatic tumor xenografts. Cancer science. 2017, 108(12):2470-7.

89. J. Incio et al., Metformin reduces desmoplasia in pancreatic cancer by reprogramming stellate cells and tumor-associated macrophages. PLOS ONE. 2015, 10, e0141392.

90. Liu, M., Jin, X., He, X., Pan, L., Zhang, X., & Zhao, Y. Macrophages Support Splenic Erythropoiesis in 4T1 Tumor-Bearing Mice. PLoS One. 2015, 10, e0121921.

91. dos S Meira, C., Gedamu L. Protective or detrimental? Understanding the role of host immunity in leishmaniasis. Microorganisms. 2019, 7(12), 695.
92. Mills C D., Ley K. M1 and M2 macrophages: the chicken and the egg of immunity. Journal of innate immunity. 2014, 6(6), 716-726.
93. Zhang L., Li Z., Skrzypczynska, K. M., Fang Q., Zhang W., O'Brien, S A., ... Yu X. Single-cell analyses inform mechanisms of myeloid-targeted therapies in colon cancer. Cell. 2020, 181(2), 442-459.
94. Azizi E., Carr A. J., Plitas G., Cornish A. E., Konopacki C., Prabhakaran S., ... Pe'er D. Single-cell map of diverse immune phenotypes in the breast tumor microenvironment. Cell. 2018, 174(5), 1293-1308.
95. Garrido-Martin E. M., Mellows T. W., Clarke J., Ganesan A. P., Wood O., Cazaly A., ... Sanchez-Elsner T. $M1^{hot}$ tumor-associated macrophages boost tissue-resident memory T cells infiltration and survival in human lung cancer. Journal for immunotherapy of cancer. 2020, 8(2).
96. Avgustinova, A., Iravani, M., Robertson, D. et al. Tumour cell-derived Wnt7a recruits and activates fibroblasts to promote tumour aggressiveness. Nat Commun. 2016, 7, 10305.
97. Koperek O., Bergner O., Pichlhöfer B., Oberndorfer F., Hainfellner J. A., Kaserer K., ... Birner P. Expression of hypoxia-associated proteins in sporadic medullary thyroid cancer is associated with desmoplastic stroma reaction and lymph node metastasis and may indicate somatic mutations in the VHL gene. The Journal of pathology. 2011, 225(1), 63-72.
98. Garrido M. C., Requena L., Kutzner H., Ortiz P., Pérez-Gómez B.,

Rodriguez-Peralto, J. L. Desmoplastic Melanoma: Expression of Epithelial–Mesenchymal Transition–Related Proteins. The American Journal of Dermatopathology. 2014, 36(3), 238-242.

99. Derksen P. W., Liu X., Saridin F., van der Gulden H., Zevenhoven J., Evers B., ... Jonkers J. Somatic inactivation of E-cadherin and p53 in mice leads to metastatic lobular mammary carcinoma through induction of anoikis resistance and angiogenesis. Cancer cell. 2006, 10(5), 437-449.

100. Shimada S., Mimata A., Sekine M., Mogushi K., Akiyama Y., Fukamachi H., ... Yuasa Y. Synergistic tumour suppressor activity of E-cadherin and p53 in a conditional mouse model for metastatic diffuse-type gastric cancer. Gut. 2014, 61(3), 344-353.

101. Sinkevicius K. W., Bellaria K. J., Barrios J., Pessina P., Gupta M., Brainson C. F., ... Kim C. F. E-cadherin loss accelerates tumor progression and metastasis in a mouse model of lung adenocarcinoma. American journal of respiratory cell and molecular biology. 2018, 59(2), 237-245.

102. Murahashi K., Yashiro M., Takenaka C., Matsuoka T., Ohira M., Hirakawa-YS Chung K. Establishment of a new scirrhous gastric cancer cell line with loss of heterozygosity at E-cadherin locus. International journal of oncology. 2001, 19(5), 1029-1033.

103. Yashiro M., Matsuoka T., Ohira M. The significance of scirrhous gastric cancer cell lines: The molecular characterization using cell lines and mouse models. Human Cell. 2018, 31, 271-281.

104. Hewitt L. C., Saito Y., Wang T., Matsuda Y., Oosting J., Silva A. N., ... Grabsch H. I. KRAS status is related to histological phenotype in gastric cancer: results from a large multicentre study. Gastric Cancer. 2019, 22, 1193-1203.

105. Smyth E. C., Nilsson M., Grabsch H. I., van Grieken N. C., Lordick F. Gastric cancer. The Lancet. 2020, 396(10251), 635-648.

106. Hu Q. P., Kuang J. Y., Yang Q. K., Bian X. W., Yu S. C. Beyond a tumor suppressor: soluble E-cadherin promotes the progression of cancer. International journal of cancer. 2016, 138(12), 2804-2812.

107. Brouxhon SM, Kyrkanides S, Teng X. Soluble E-cadherin: a critical oncogene modulating receptor tyrosine kinases, MAPK and PI3K/Akt/mTOR signaling. Oncogene. 2014, 33:225–35.

108. Sukri A., Hanafiah A., Kosai N. R. The roles of immune cells in gastric cancer: anti-cancer or pro-cancer? Cancers. 2022, 14(16), 3922.

109. Pernot S. Terme M. Radosevic-Robin N. Castan F. Badoual C. Marcheteau E. Penault-Llorca F. Bouche O. Bennouna J. Francois E. Infiltrating and peripheral immune cell analysis in advanced gastric cancer according to the Lauren classification and its prognostic significance. Gastric Cancer. 2020, 23, 73–81.

110. Hermans F., Hemeryck L., Lambrichts I., Bronckaers A., & Vankelecom H. Intertwined signaling pathways governing tooth development: a give-and-take between canonical Wnt and Shh. Frontiers in cell and Developmental biology. 2021, 9, 758203.

111. Iwatsuki K., Liu H. X., Grónder A., Singer M. A., Lane T. F., Grosschedl R., ... Margolskee R. F. Wnt signaling interacts with Shh to regulate taste papilla development. Proceedings of the National Academy of Sciences. 2007 104(7), 2253-2258.

112. Bailey J. M., Swanson B. J., Hamada T., Eggers J. P., Singh P. K., Caffery T., ... Hollingsworth M. A. Sonic hedgehog promotes

desmoplasia in pancreatic cancer. Clinical cancer research. 2008, 14(19), 5995-6004.

113. Tian H., Callahan C. A., DuPree K. J., Darbonne W. C., Ahn C. P., Scales S. J., de Sauvage F. J. Hedgehog signaling is restricted to the stromal compartment during pancreatic carcinogenesis. Proceedings of the National Academy of Sciences. 2009, 106(11), 4254-4259.

114. Olive K. P., Jacobetz M. A., Davidson C. J., Gopinathan A., McIntyre D., Honess D., ... Tuveson, D. A. Inhibition of Hedgehog signaling enhances delivery of chemotherapy in a mouse model of pancreatic cancer. Science. 2009, 324(5933), 1457-1461.

Abstract in Korean

E-Cadherin 돌연변이 상태에 따른 위 종양 모델의 표현형 분석

서울대학교 대학원
의과학과 의과학전공
박기석

위암은 전세계적으로 높은 사망률을 보이는 주요 질병 중 하나로, 화학요법, 면역요법, 면역관문억제제 등의 치료 전략이 존재하지만, 종양내 미세환경을 포함한 다양한 요소에 의해 제한적인 약효성을 보인다. CDH1은 E-Cadherin을 암호화하는 유전자로, 미만형 위암 환자에서 빈번한 돌연변이를 보이는데, 미만형 위암은 낮은 치료 반응률을 포함하여 부정적인 예후를 보이는 것으로 알려져 있다. 이 연구에서는 두 마우스 유래 위암, Tcon과 Dcon 종양의 표현형적 차이에 대해 연구하였다. Tcon은 종양내 미세환경의 과도한 콜라겐 섬유의 축적으로 인해 심각한 종양섬유화가 발생하여 경도가 높은 종양체를 형성하였다. 종양섬유화는 암-연관 섬유아세포에 의해 촉진되는 것으로 알려져 있으며, 종양진행 및 약물 전달 억제에 기여한다. 정밀한 유세포 분석을 통해, 종양 섬유화에 기여하는 αSMA 단일-양성 암-연관 섬유아세포와 면역억제기전에 중요한 기능을 수행할 수 있을 것으로 추측되는 PD-L1을 발현하는 암-연관 섬유아세포가 Tcon 종양에서 Dcon 종양에 비해 높은 비율로 포진함을 알 수 있었다. 또한, Tcon 종양의 경우, Dcon 종양에 비해 종양내 혈관의 발달이 부진하였으며, 낮은 약물 전달률로 인한 치료 반응률의 저하가 예상되었다. 반면, Dcon 종양의 경우, T 세포를 포함한 각

종 면역세포의 침습 또한 Tcon 종양에 비해 높은 수준으로 이루어짐을 확인할 수 있었으며, 특히 T 세포 중 TNFα, Granzyme B, Perforin, Interferon-γ와 같은 항-종양성 사이토카인을 생산하는 비율이 높아, 항-종양성 면역체계가 보다 활성화되었음을 알 수 있었다. 추가적으로, Dcon 종양을 이식한 마우스는 종양으로 인해 발생한 빈혈과 더불어 비장의 비대화를 보였으며, 비장 내부에서는 골수성 면역세포와 적아세포의 비정상적인 증식을 확인할 수 있었는데, 이러한 세포들은 종양 내부로 침습하여 면역억제기전 및 친종양성 기능을 수행할 것으로 기대된다. 위와 같은 연구를 통해 두 종류의 위 종양의 표현형적 특징에 대한 통찰을 제공할 수 있었으며, 더불어 임상 적용으로의 가능성을 제시함으로써 위암 환자의 치료 접근성을 향상시킬 수 있었다.

주요어 : 위암, 종양섬유화, 암-연관 섬유아세포, 종양내혈관, 비장 비대증
학번 : 2021-23200